



**HAL**  
open science

# Quantum surface effects in the electromagnetic coupling between a quantum emitter and a plasmonic nanoantenna: time-dependent density functional theory vs. semiclassical Feibelman approach

Antton Babaze, Eduardo Ogando, P. Elli Stamatopoulou, Christos Tserkezis, N. Asger Mortensen, Javier Aizpurua, Andrei Borisov, Ruben Esteban

## ► To cite this version:

Antton Babaze, Eduardo Ogando, P. Elli Stamatopoulou, Christos Tserkezis, N. Asger Mortensen, et al.. Quantum surface effects in the electromagnetic coupling between a quantum emitter and a plasmonic nanoantenna: time-dependent density functional theory vs. semiclassical Feibelman approach. *Optics Express*, 2022, 30 (12), pp.21159-21183. 10.1364/OE.456338 . hal-03690217

**HAL Id: hal-03690217**

**<https://hal.science/hal-03690217v1>**







Submitted on 8 Jun 2022

**HAL** is a multi-disciplinary open access archive for the deposit and dissemination of scientific research documents, whether they are published or not. The documents may come from teaching and research institutions in France or abroad, or from public or private research centers.

L'archive ouverte pluridisciplinaire **HAL**, est destinée au dépôt et à la diffusion de documents scientifiques de niveau recherche, publiés ou non, émanant des établissements d'enseignement et de recherche français ou étrangers, des laboratoires publics ou privés.



# Quantum surface effects in the electromagnetic coupling between a quantum emitter and a plasmonic nanoantenna: time-dependent density functional theory vs. semiclassical Feibelman approach

ANTTON BABAZE,<sup>1,2,7</sup>  EDUARDO OGANDO,<sup>3</sup>  
P. ELLI STAMATOPOULOU,<sup>4</sup>  CHRISTOS TSERKEZIS,<sup>4</sup>   
N. ASGER MORTENSEN,<sup>4,5</sup>  JAVIER AIZPURUA,<sup>1,2</sup>   
ANDREI G. BORISOV,<sup>6</sup>  AND RUBEN ESTEBAN<sup>1,2,8</sup>

<sup>1</sup>Materials Physics Center CSIC-UPV/EHU, Paseo Manuel de Lardizabal 5, 20018 Donostia-San Sebastián, Spain

<sup>2</sup>Donostia International Physics Center DIPC, Paseo Manuel de Lardizabal 4, 20018 Donostia-San Sebastián, Spain

<sup>3</sup>Department of Physics, University of the Basque Country UPV/EHU, Paseo de la Universidad 7, 01006 Vitoria-Gasteiz, Spain

<sup>4</sup>Center for Nano Optics, University of Southern Denmark, Campusvej 55, DK-5230 Odense M, Denmark

<sup>5</sup>Danish Institute for Advanced Study, University of Southern Denmark, Campusvej 55, DK-5230 Odense M, Denmark

<sup>6</sup>Institut des Sciences Moléculaires d'Orsay, UMR 8214 CNRS-Université Paris-Saclay, Bât. 520, 91405 Orsay Cedex, France

<sup>7</sup>anttonbabaze@dipc.org

<sup>8</sup>ruben.esteban@ehu.eus

**Abstract:** We use time-dependent density functional theory (TDDFT) within the jellium model to study the impact of quantum-mechanical effects on the self-interaction Green's function that governs the electromagnetic interaction between quantum emitters and plasmonic metallic nanoantennas. A semiclassical model based on the Feibelman parameters, which incorporates quantum surface-response corrections into an otherwise classical description, confirms surface-enabled Landau damping and the spill out of the induced charges as the dominant quantum mechanisms strongly affecting the nanoantenna–emitter interaction. These quantum effects produce a redshift and broadening of plasmonic resonances not present in classical theories that consider a local dielectric response of the metals. We show that the Feibelman approach correctly reproduces the nonlocal surface response obtained by full quantum TDDFT calculations for most nanoantenna–emitter configurations. However, when the emitter is located in very close proximity to the nanoantenna surface, we show that the standard Feibelman approach fails, requiring an implementation that explicitly accounts for the nonlocality of the surface response in the direction parallel to the surface. Our study thus provides a fundamental description of the electromagnetic coupling between plasmonic nanoantennas and quantum emitters at the nanoscale.

© 2022 Optica Publishing Group under the terms of the [Optica Open Access Publishing Agreement](#)

## 1. Introduction

Due to the excitation of localized surface plasmons, metallic nanoparticles strongly enhance the amplitude of the incident light and confine the electromagnetic field well below the diffraction limit, thus acting as optical nanoantennas [1]. When a quantum emitter (QE), such as an organic

molecule or a quantum dot, is placed close to a plasmonic nanoantenna, the absorption and emission rate of the QE is greatly increased, leading to a plethora of interesting phenomena [2–7]. For example, the spontaneous decay rate and exciton energy of the QE are drastically modified, and hybrid plasmon–exciton polaritonic states can be created in the strong-coupling regime [8–13]. The coupling between QEs and plasmonic nanoantennas has been extensively used in a variety of applications, such as in surface-enhanced fluorescence [14–16], biosensing [17,18], or single-molecule detection [19,20], among others.

Together with the experimental progress, considerable theoretical effort has been devoted to accurately describing the electromagnetic interaction between a QE and a nanoantenna, and several models at different levels of approximation have been adopted [21–25]. An approach often used to model the exciton dynamics in the QE is the point-dipole approximation, which describes the QE as a structureless two-level electronic system under weak illumination [26–29]. Despite its simplicity, the point-dipole approximation is found to properly describe typical situations where the spatial extent of the QE is much smaller than the effective field localization of the plasmonic resonance and the electronic orbitals of the QE and those of the metal atoms forming the nanoantenna do not spatially overlap. Indeed, in such situations, the spatial variation of the electric field and the actual electronic structure of the QE [30–34] or charge-transfer processes related to electron tunneling [35–38] have almost no effect in the optical nanoantenna–QE coupling.

Within the point-dipole approximation, the electromagnetic coupling between a QE and a nanoantenna can be described by the dyadic Green’s function,  $\hat{G}(\mathbf{r}, \mathbf{r}_{\text{QE}}, \omega)$  [26,34,39–42], which provides the electric field induced by a metallic nanoantenna at a position  $\mathbf{r}$  in response to the electromagnetic radiation of a point dipole located at  $\mathbf{r}_{\text{QE}}$  oscillating at frequency  $\omega$ . In the weak nanoantenna–QE coupling regime, the *self-interaction* given by  $\hat{G}(\mathbf{r} = \mathbf{r}_{\text{QE}}, \mathbf{r}_{\text{QE}}, \omega)$  determines the enhancement of the total decay rate of the QE (Purcell effect, [43]) and the change of its resonant energy (Lamb shift) produced by the plasmonic environment.

A proper description of the self-interaction Green’s function requires a realistic model for the optical response of metals. To this end, a local dielectric function obtained experimentally or from simple theoretical models is commonly used. However, such a dielectric function does not include quantum phenomena relevant in plasmonic nanoantennas, such as electron spill-out, Landau damping, finite-size effects, electron tunneling and nonlocal dynamical screening [44–52]. These nonclassical phenomena, inherent to the quantum nature of electrons in metals, have greater impact when reducing the characteristic dimensions of the system, e.g. the size of the metallic nanoparticles, the gap separation in nanoparticle ensembles, or the nanoantenna–QE distance. Quantum effects become particularly important in systems with characteristic dimensions below  $\sim 10$  nm [53–55].

In this context, diverse *semiclassical* models have been developed to partially account for certain nonclassical effects [56]. For example, some of these approaches introduce the intrinsic nonlocality of the metals by combining classical electrodynamics and hydrodynamic descriptions of the induced charges with the use of phenomenological parameters [57–72]. Moreover, other semiclassical descriptions account for the spill-out of the induced electron density and Landau damping by incorporating *ab initio* quantum surface-response corrections at the metal–dielectric boundaries in the solution of Maxwell’s equations. This can be achieved thanks to the use of the so-called Feibelman parameters obtained from quantum calculations [73–81]. By means of these approaches, it has been predicted that nonclassical phenomena can substantially influence the optical nanoantenna–QE interaction [55,82–90]. However, fully quantum calculations of representative systems, based e.g. on the time-dependent density functional theory (TDDFT), are often required to ensure that all the quantum effects affecting the interaction are correctly described and to establish the validity of the different semiclassical models.

In this work, we use a many-body quantum approach, within the Kohn–Sham (KS) scheme of TDDFT (widely used for plasmonic systems [91–101]), to study the coupling between canonical metallic nanoantennas and QEs. The nanoantenna–QE separations are set sufficiently large so that electron tunneling is negligible and the electromagnetic interaction determines the optical properties of the system. However, we consider nanoantenna–QE separations small enough for other quantum phenomena such as nonlocality to be important. Without any aprioristic assumption, we calculate the self-interaction Green’s function  $\hat{G}(\mathbf{r}_{\text{QE}}, \mathbf{r}_{\text{QE}}, \omega)$  that governs the nanoantenna–QE coupling. A comparison with classical results obtained within the local-response approximation (LRA) reveals the importance of quantum effects. Further, the comparison between the TDDFT results and a semiclassical nonlocal model that incorporates quantum surface-response corrections *via* the Feibelman parameters serves to identify surface-enabled Landau damping and spill-out of the induced electron density as the dominant quantum mechanisms dramatically influencing the electromagnetic nanoantenna–QE interaction.

TDDFT also provides a benchmark to establish the validity range of the standard implementation of the semiclassical Feibelman formalism to adequately account for the dominant quantum phenomena arising in the electromagnetic interaction between a QE and a nanoantenna. The standard Feibelman approach, as used here, neglects the nonlocal surface response in the direction parallel to the surface (long-wavelength limit), enabling an efficient implementation of nonlocality in nanoscale geometries [79]. Here we identify situations of very small nanoantenna–QE distance where the standard implementation of the Feibelman approach eventually fails, indicating that the dispersion of the Feibelman parameters with respect to the wavenumber parallel to the surface needs to be considered.

Atomic units (au) are used throughout the text unless otherwise stated.

## 2. System and methods

We analyze the electromagnetic coupling between a point-like QE and two different canonical metallic nanoantennas. First, we consider in Sections 3.1, 3.2, and 3.3 the case of a single spherical nanoparticle, where the QE is placed at a distance  $d$  from the nanoparticle surface (Fig. 1(a)). Then, in Section 3.4, we analyze a metallic dimer composed by two identical spherical nanoparticles separated by a gap of size  $D$  (Fig. 1(b)). The QE is situated at the center of the gap ( $z = 0$ ). We define the coordinates such that the center of the nanoparticle(s) is at the  $z$ -axis. The entire system is surrounded by vacuum.

We consider closed-shell free-electron (jellium) metal nanoparticles. The radius of the nanoparticles is  $a = 65.83 a_0$  ( $\approx 3.5$  nm), which guarantees a well-developed plasmonic response [102] in the TDDFT simulations ( $a_0 = 0.053$  nm is the Bohr radius). The surface-to-emitter distance is sufficiently large to ensure that the electron densities of the metallic nanoparticles at the position of the QE are negligible, and therefore there is no electron tunneling [54,103–107]. Specifically, we consider surface-to-emitter distances  $d$  in the range of  $d = 10 - 42 a_0$  ( $\approx 0.5 - 2.2$  nm) for the case of the single nanoantenna, and gap separations of  $D = 2d = 20 - 45 a_0$  ( $\approx 1.1 - 2.4$  nm) for the dimer structure. We use the point-dipole approximation to model the QE and thus neglect its spatial extent.

We focus on the study of  $\hat{G}(\mathbf{r}_{\text{QE}}, \mathbf{r}_{\text{QE}}, \omega)$ , which provides the electric field  $\mathbf{E}(\mathbf{r}_{\text{QE}}, \omega)$  created by the metallic nanoantenna at a position  $\mathbf{r}_{\text{QE}}$  in response to a point dipole  $\mathbf{p}_d$  located at the same position,

$$\mathbf{E}(\mathbf{r}_{\text{QE}}, \omega) = \hat{G}(\mathbf{r}_{\text{QE}}, \mathbf{r}_{\text{QE}}, \omega) \cdot \mathbf{p}_d, \quad (1)$$

where  $\omega$  is the resonant frequency of the QE. We refer to  $\hat{G}(\mathbf{r}_{\text{QE}}, \mathbf{r}_{\text{QE}}, \omega)$  as the *self-interaction* Green’s function. Notice that the definition of  $\hat{G}(\mathbf{r}_{\text{QE}}, \mathbf{r}_{\text{QE}}, \omega)$  given by Eq. (1) differs from that used in other works [108] by a factor  $1/(\omega^2 \mu_0)$  in SI units (with  $\mu_0$  the vacuum permeability), and that  $\hat{G}(\mathbf{r}_{\text{QE}}, \mathbf{r}_{\text{QE}}, \omega)$  only considers the electric field reflected by the metallic nanoantenna (and not the one induced by the isolated QE).

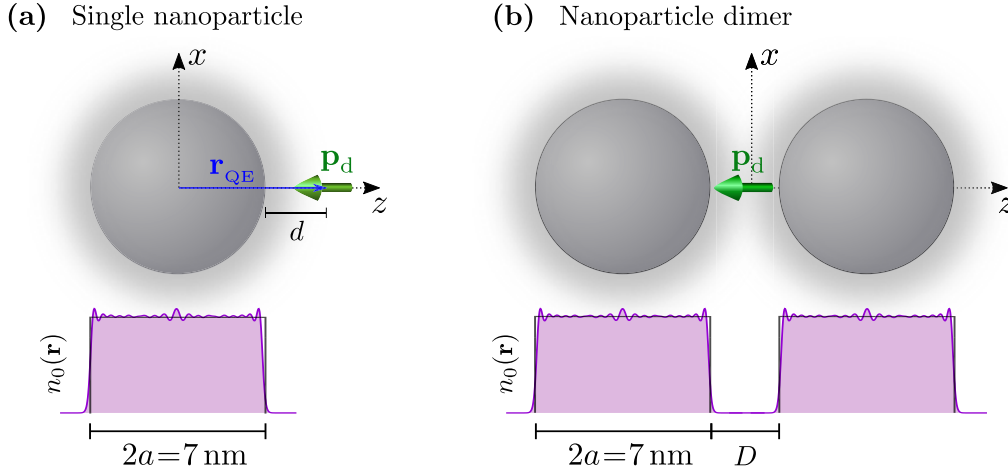


**Fig. 1.** Sketch of the studied systems, consisting of a QE modeled as a point dipole  $\mathbf{p}_d$  placed (a) at a distance  $d$  from the surface of a single spherical metallic nanoparticle, and (b) at the center of a gap of size  $D$  formed by two identical spherical metallic nanoparticles. The point dipole is oriented along the  $z$ -axis, which is also the axis of the dimer. Each nanoparticle is represented within the free-electron (jellium) model and contains 4458 conduction electrons, resulting in a radius  $a = 65.83 a_0 (\approx 3.5 \text{ nm})$ . The calculated ground-state electron density of the nanoparticles,  $n_0(\mathbf{r})$ , is represented by the fuchsia filled-line, and the gray line represents the background jellium edge considered in the classical LRA calculations.

Importantly,  $\hat{\mathbf{G}}(\mathbf{r}_{\text{QE}}, \mathbf{r}_{\text{QE}}, \omega)$  determines the total decay rate ( $\Gamma$ ) and the Lamb shift ( $\Delta\omega$ ) of a QE that interacts weakly with the plasmonic nanoantenna [34,40–42],

$$\Gamma = \gamma_0 + \gamma_{\text{QE}}^{\text{nr}} + 2|\mu|^2 \text{Im}\{\hat{\mathbf{k}} \cdot \hat{\mathbf{G}}(\mathbf{r}_{\text{QE}}, \mathbf{r}_{\text{QE}}, \omega) \cdot \hat{\mathbf{k}}\}, \quad (2a)$$

$$\Delta\omega = -|\mu|^2 \text{Re}\{\hat{\mathbf{k}} \cdot \hat{\mathbf{G}}(\mathbf{r}_{\text{QE}}, \mathbf{r}_{\text{QE}}, \omega) \cdot \hat{\mathbf{k}}\}, \quad (2b)$$

with  $\gamma_0$ ,  $\gamma_{\text{QE}}^{\text{nr}}$  and  $\mu$  being the spontaneous decay rate in vacuum, the non-radiative intrinsic loss rate, and the transition dipole moment of the QE along the  $\hat{\mathbf{k}}$ -direction, respectively [108]. The unit-length vector  $\hat{\mathbf{k}}$  defines the orientation of  $\mathbf{p}_d$ . We note that the enhancement of the decay rate due to the nanoantenna–QE coupling is often normalized by  $\gamma_0$ , which gives the Purcell factor

$$F_P = \frac{\Gamma - \gamma_{\text{QE}}^{\text{nr}}}{\gamma_0} = 1 + \frac{3c^3}{2\omega^3} \text{Im}\{\hat{\mathbf{k}} \cdot \hat{\mathbf{G}}(\mathbf{r}_{\text{QE}}, \mathbf{r}_{\text{QE}}, \omega) \cdot \hat{\mathbf{k}}\}, \quad (3)$$

$c$  being the speed of light in vacuum [109,110].

We restrict our analysis to the case of a point dipole oriented along the  $z$ -axis,  $\mathbf{p}_d = p_d \hat{\mathbf{z}}$ , where  $\hat{\mathbf{z}}$  is the unit-length vector along the  $z$ -axis. Moreover, we use  $\mathbf{r}_{\text{QE}} = r_{\text{QE}} \hat{\mathbf{z}}$ , so that  $\hat{\mathbf{G}}(\mathbf{r}_{\text{QE}}, \mathbf{r}_{\text{QE}}, \omega)$  can be considered as a scalar,  $\hat{\mathbf{G}}(\mathbf{r}_{\text{QE}}, \mathbf{r}_{\text{QE}}, \omega) \equiv G(\mathbf{r}_{\text{QE}}, \mathbf{r}_{\text{QE}}, \omega)$ , because of the symmetry. Retardation effects are neglected due to the small size of the system. In the upcoming subsections, we briefly explain the three different models used in this work to obtain  $G(\mathbf{r}_{\text{QE}}, \mathbf{r}_{\text{QE}}, \omega)$ , namely the TDDFT, the classical LRA, and the semiclassical model based on the Feibelman parameter.

### 2.1. Time-dependent density functional theory (TDDFT)

The electronic structure of the nanoantennas is described in the TDDFT calculations within the jellium model of free-electron metals [111,112], where the ions at the lattice sites are modeled as

a uniform positive charge with density

$$n_+ = \left( \frac{4}{3} \pi r_s^3 \right)^{-1} \quad (4)$$

distributed over the spatial extent of the nanostructures. We use a Wigner–Seitz radius equal to that of sodium,  $r_s = 4 a_0$ , which allows us to use the values of the Feibelman parameters calculated in recent works for that material [78] when comparing with the semiclassical theory. Note also that the dipolar plasmon frequency of sodium nanoparticles lies at optical frequencies, very close to that of gold nanoparticles, thus placing the results within the frequency range relevant for actual applications in plasmonics. The closed-shell nanoparticles contain 4458 conduction electrons, which sets the radius of the background jellium edge to  $a = 65.83 a_0$  ( $\approx 3.5$  nm). As compared to fully atomistic descriptions, the jellium model allows us to tackle nanoparticles of larger size so that the plasmonic excitations are well developed.

We first calculate the electron density  $n_0(\mathbf{r})$  of the system in the ground-state configuration within static density functional theory (DFT) [113,114],

$$n_0(\mathbf{r}) = \sum_{j \in \text{occ}} \chi_j |\Psi_j^0(\mathbf{r})|^2, \quad (5)$$

where  $\chi_j$  accounts for spin and symmetry degeneracy, and the summation runs over the occupied ( $j \in \text{occ}$ ) ground-state KS orbitals,  $\Psi_j^0(\mathbf{r})$ . The equilibrium electron density  $n_0(\mathbf{r})$  of the metallic nanoantennas shown in Figs. 1(a-b) (fuchsia filled curves) nicely illustrates quantum phenomena such as electron spill-out and Friedel oscillations [115,116]. Details on the self-consistent ground-state calculations for both the single and the dimer structures can be found in prior works [117].

In order to obtain the self-interaction Green's function,  $G_{\text{TDDFT}}(\mathbf{r}_{\text{QE}}, \mathbf{r}_{\text{QE}}, \omega)$ , we solve the time-dependent KS equations of TDDFT for the occupied KS orbitals  $\Psi_j(\mathbf{r}, t)$ ,

$$i \frac{\partial}{\partial t} \Psi_j(\mathbf{r}, t) = \hat{H}[n](\mathbf{r}, t) \Psi_j(\mathbf{r}, t), \quad (6)$$

where the Hamiltonian

$$\hat{H}[n] = \hat{T} + V_{\text{h}}[n](\mathbf{r}, t) + V_{\text{xc}}[n](\mathbf{r}, t) - V_{\text{ext}}(\mathbf{r}, t), \quad (7)$$

is a functional of the time-dependent electron density,

$$n(\mathbf{r}, t) = \sum_{j \in \text{occ}} \chi_j |\Psi_j(\mathbf{r}, t)|^2. \quad (8)$$

In Eq. (7), the kinetic-energy operator is given by  $\hat{T} = -\frac{1}{2} \nabla^2$ . Since the size of the considered systems is much smaller than the relevant optical wavelengths, retardation effects are neglected. The Hartree potential  $V_{\text{h}}$  is then obtained from Poisson's equation,  $\nabla^2 V_{\text{h}}(\mathbf{r}, t) = -4\pi (n(\mathbf{r}, t) - n_+)$ , and the exchange–correlation potential  $V_{\text{xc}}[n](\mathbf{r}, t)$  is calculated using the functional of Gunnarsson and Lundqvist [118] within the adiabatic local-density approximation (ALDA) [113,119].  $V_{\text{ext}}(\mathbf{r}, t)$  is an impulsive potential created by a point dipole of sufficiently small amplitude  $p_{\text{d}}$  to ensure a linear response,

$$V_{\text{ext}}(\mathbf{r}, t) = p_{\text{d}} \hat{\mathbf{z}} \cdot \frac{\mathbf{r} - \mathbf{r}_{\text{QE}}}{|\mathbf{r} - \mathbf{r}_{\text{QE}}|^3} \delta(t), \quad (9)$$

with  $\delta(t)$  the Dirac delta function.  $V_{\text{ext}}(\mathbf{r}, t)$  appears with a minus sign in the Hamiltonian  $\hat{H}[n]$  given by Eq. (7) because  $V_{\text{ext}}(\mathbf{r}, t)$  is applied to electrons with charge  $q_e = -1$ . The initial



conditions in Eq. (6) are given by the ground-state KS orbitals,  $\Psi_j(\mathbf{r}, t = 0) \equiv \Psi_j^0(\mathbf{r})$ . Short time-step propagation algorithms based on Split-Operator techniques are used to solve Eq. (6) in real time [120], with the orbitals  $\Psi_j(\mathbf{r}, t)$  represented on a spatially-discretized grid using a spacing of  $\sim 0.35 a_0$ . For the single nanoparticle we use a spherical mesh, whereas for the dimer we adopt cylindrical coordinates. Both single and dimer antenna geometries possess rotational symmetry with respect to the  $z$ -axis, which strongly reduces the computational load. The propagation time-step is typically  $\Delta t \sim 0.05$  au.

From the time-dependent electron density  $n(\mathbf{r}, t)$  obtained by solving Eqs. (6)–(8) self-consistently, we calculate the time-dependent electric field  $\tilde{\mathbf{E}}(\mathbf{r} = \mathbf{r}_{\text{QE}}, t)$  induced by the metallic nanostructure at the position  $\mathbf{r}_{\text{QE}}$  of the QE,

$$\tilde{\mathbf{E}}(\mathbf{r} = \mathbf{r}_{\text{QE}}, t) = \nabla V_{\text{h}}[n](\mathbf{r} = \mathbf{r}_{\text{QE}}, t). \quad (10)$$

$\tilde{\mathbf{E}}(\mathbf{r}_{\text{QE}}, t) = \tilde{E}(\mathbf{r}_{\text{QE}}, t) \hat{\mathbf{z}}$  is oriented along the  $z$ -axis due to the symmetry of the system.

Finally, by using the time-to-frequency Fourier transform, we obtain the frequency-resolved self-interaction Green's function [121],

$$G_{\text{TDDFT}}(\mathbf{r}_{\text{QE}}, \mathbf{r}_{\text{QE}}, \omega) = \frac{1}{p_{\text{d}}} \underbrace{\int_0^{T_{\text{f}}} dt \tilde{E}(\mathbf{r}_{\text{QE}}, t) e^{i(\omega + i\eta/2)t}}_{E(\mathbf{r}_{\text{QE}}, \omega)}, \quad (11)$$

where  $T_{\text{f}} = 3500$  au is the total propagation time used in our simulations (enough to achieve convergence), and  $\eta = 0.07$  eV accounts for relaxation processes beyond the (ALDA) TDDFT description of the many-body dynamics such as the interaction of excited electrons with phonons and many-body inelastic electron–electron scattering events [122,123].

## 2.2. Classical local-response approximation (LRA)

The classical nonretarded self-interaction Green's function is obtained in the frequency domain from the electrostatic potential  $V_{\text{ind}}(\mathbf{r}, \omega)$  induced by the metallic nanostructure in response to the external excitation  $V_{\text{ext}}(\mathbf{r}, \omega)$  of a point dipole oscillating at a transition frequency  $\omega$ ,

$$V_{\text{ext}}(\mathbf{r}, \omega) = p_{\text{d}} \hat{\mathbf{z}} \cdot \frac{\mathbf{r} - \mathbf{r}_{\text{QE}}}{|\mathbf{r} - \mathbf{r}_{\text{QE}}|^3}. \quad (12)$$

The induced potential  $V_{\text{ind}}(\mathbf{r}, \omega)$  satisfies Laplace's equation

$$\nabla^2 V_{\text{ind}}(\mathbf{r}, \omega) = 0. \quad (13)$$

Within the LRA, results are obtained by applying the standard hard-wall boundary conditions at the metal–vacuum interfaces,

$$\begin{aligned} \hat{\mathbf{n}} \times (\mathbf{E}_{\text{LRA}}^{\text{out}} - \mathbf{E}_{\text{LRA}}^{\text{in}}) &= 0, \\ \hat{\mathbf{n}} \cdot (\mathbf{D}_{\text{LRA}}^{\text{out}} - \mathbf{D}_{\text{LRA}}^{\text{in}}) &= 0, \end{aligned} \quad (14)$$

and using a Drude-type local dielectric function to characterize the metal,

$$\varepsilon_m(\omega) = 1 - \frac{\omega_p^2}{\omega^2 + i\gamma_p\omega}. \quad (15)$$

In Eq. (14), the superscript ‘in’ defines the fields within the region inside the metal while the superscript ‘out’ those in the surrounding vacuum, and  $\hat{\mathbf{n}}$  is the normal unit vector pointing outwards from the metal boundary.  $\mathbf{E}_{\text{LRA}}(\mathbf{r}, \omega) = -\nabla (V_{\text{ext}}(\mathbf{r}) + V_{\text{ind}}(\mathbf{r}, \omega))$  is the total electric

field, and  $\mathbf{D}_{\text{LRA}}(\mathbf{r}, \omega) = \varepsilon(\mathbf{r}, \omega)\mathbf{E}_{\text{LRA}}(\mathbf{r}, \omega)$  is the electric displacement field in a medium with dielectric function  $\varepsilon(\mathbf{r}, \omega)$ . The boundary conditions given by Eq. (14) are consistent with the polarization charges being located strictly at the metal boundary. In this work, the plasma frequency  $\omega_p = \sqrt{\frac{3}{r_s}} = 5.89$  eV and the intrinsic damping parameter  $\gamma_p = 0.1$  eV are used in Eq. (15). The value of parameter  $\gamma_p$  is obtained from the comparison of the absorption spectrum of a single spherical nanoantenna calculated with TDDFT and with the semiclassical model, as explained in Appendix A. In the case of a point-like QE at position  $\mathbf{r}_{\text{QE}}$  exciting the single spherical nanoparticle of radius  $a$ , Eqs. (13)–(14) can be solved analytically, and the self-interaction Green's function reads [21]

$$G_{\text{LRA}}(\mathbf{r}_{\text{QE}}, \mathbf{r}_{\text{QE}}, \omega) = -\nabla V_{\text{ind}}(\mathbf{r} = \mathbf{r}_{\text{QE}}, \omega) = \sum_{\ell=1}^{\infty} (\ell + 1)^2 \frac{a^{2\ell+1}}{R^{2\ell+4}} \frac{\varepsilon_m(\omega) - 1}{\varepsilon_m(\omega) + \frac{\ell+1}{\ell}}, \quad (16)$$

with  $R$  the distance between the position  $\mathbf{r}_{\text{QE}}$  of the QE and the center of the nanoparticle and  $\ell$  the multipole order of the plasmonic resonance. The numerical implementation used to solve Eqs. (13)–(14) for the dimer structure is based on a coupled-multipole method [124,125], which uses the solution of the individual spherical nanoparticles. Details can be found in Ref. [38].

### 2.3. Semiclassical Feibelman approach

The semiclassical nonlocal model employed here is based on the Feibelman surface-response function  $d_{\perp}(\omega)$  [73–75], a (frequency-dependent) complex-valued function that accounts for the position of the centroid of the induced charges with respect to the positive background edge of the nanoparticles. For a more complete picture, one could also include another parameter,  $d_{\parallel}(\omega)$ , related to the parallel component of the induced current at the metallic surface. However,  $d_{\parallel}(\omega)$  vanishes for charge-neutral planar surfaces [55,78], and for curved surfaces  $d_{\parallel}(\omega)$  is expected to be much less important than  $d_{\perp}(\omega)$  [75]. Therefore, in this work we consider  $d_{\parallel}(\omega) = 0$ .

The parameter  $d_{\perp}(\omega)$  incorporates important quantum-mechanical effects, since its real and imaginary parts are related to the spill-out of dynamical screening charges and surface-enabled Landau damping, respectively. Moreover, as the  $d_{\perp}(\omega)$  parameter is typically extracted from TDDFT calculations that inherently account for the finite compressibility of the electron gas, the Feibelman model also incorporates nonlocal effects of the electron dynamics in bulk [56]. This  $d_{\perp}(\omega)$  parameter, usually obtained for a planar metal–vacuum interface, has been widely used to address the optical response of arbitrary-shaped metallic nanostructures [55,78,90,126]. The current implementation of the  $d_{\perp}(\omega)$  parameter neglects the nonlocality of the metal response in the direction parallel to the surface (long-wavelength limit). This is a reasonable approximation when the radius of curvature of the nanostructure or the typical length of the variation of the external potential along the surface is much larger than the Fermi wavelength. One of the objectives of the present work is indeed to test the validity of the above approach for situations where the radius of curvature of the system is small and the external potential along the metal surface (here created by the point-dipole QE) varies rapidly.

In brief, the Feibelman model is an extension of the classical LRA that allows us to account for the smooth variation of the induced electron density across the metal–vacuum interface. Within this semiclassical approach, the self-interaction Green's function is also obtained from the electrostatic potential  $V_{\text{ind}}(\mathbf{r}, \omega)$  (Eq. (13)) with the use of a Drude-type local dielectric function  $\varepsilon_m(\omega)$  (Eq. (15)). However, in contrast with the hard-wall boundary conditions applied at the metal–vacuum interface within the classical LRA, here we use the following expressions obtained in Ref. [79],

$$\begin{aligned} \hat{\mathbf{n}} \times (\mathbf{E}_{\text{F}}^{\text{out}} - \mathbf{E}_{\text{F}}^{\text{in}}) &= -d_{\perp}(\omega) \hat{\mathbf{n}} \times \nabla \left[ \hat{\mathbf{n}} \cdot (\mathbf{E}_{\text{F}}^{\text{out}} - \mathbf{E}_{\text{F}}^{\text{in}}) \right], \\ \hat{\mathbf{n}} \cdot (\mathbf{D}_{\text{F}}^{\text{out}} - \mathbf{D}_{\text{F}}^{\text{in}}) &= d_{\parallel}(\omega) \nabla \cdot \left[ \hat{\mathbf{n}} \times (\mathbf{D}_{\text{F}}^{\text{out}} - \mathbf{D}_{\text{F}}^{\text{in}}) \right], \end{aligned} \quad (17)$$



where the subscript ‘F’ denotes that the fields are calculated within the Feibelman model. As mentioned above, in this work we consider  $d_{\parallel}(\omega) = 0$  and use the  $d_{\perp}(\omega)$  function obtained by Christensen *et al.* [78] within the jellium model (Na,  $r_s = 4 a_0$ ) for a semi-infinite planar metal surface (see also Ref. [55]).

Similarly to the classical LRA, using the Feibelman model one obtains an analytical solution of the potential  $V_{\text{ind}}(\mathbf{r}, \omega)$  induced by a single spherical nanoantenna of radius  $a$  in response to the point-dipole excitation. The resulting nonretarded self-interaction Green’s function for  $d_{\parallel}(\omega) = 0$  is given by [55,75]

$$G_{\text{F}}(\mathbf{r}_{\text{QE}}, \mathbf{r}_{\text{QE}}, \omega) = \sum_{\ell=1}^{\infty} (\ell + 1)^2 \frac{a^{2\ell+1}}{R^{2\ell+4}} \frac{(\varepsilon_m(\omega) - 1) \left(1 + \frac{\ell}{a} d_{\perp}(\omega)\right)}{\varepsilon_m(\omega) + \frac{\ell+1}{\ell} - (\varepsilon_m(\omega) - 1) \frac{\ell+1}{a} d_{\perp}(\omega)}. \quad (18)$$

For  $d_{\perp}(\omega)/a \rightarrow 0$ , i.e., for situations where the radius of the nanoparticle  $a$  is much larger than the surface-response correction  $d_{\perp}(\omega)$ , Eq. (18) reduces to the classical LRA expression of  $G_{\text{LRA}}(\mathbf{r}_{\text{QE}}, \mathbf{r}_{\text{QE}}, \omega)$  given by Eq. (16).

For the dimer structure, we extend the numerical method used for the classical LRA [38] so as to account for the modified boundary conditions given by Eq. (17) (see further details in Appendix B). For simplicity, in the following we generically use  $G(\mathbf{r}_{\text{QE}}, \mathbf{r}_{\text{QE}}, \omega)$  to refer to any of  $G_{\text{TDDFT}}(\mathbf{r}_{\text{QE}}, \mathbf{r}_{\text{QE}}, \omega)$ ,  $G_{\text{LRA}}(\mathbf{r}_{\text{QE}}, \mathbf{r}_{\text{QE}}, \omega)$  and  $G_{\text{F}}(\mathbf{r}_{\text{QE}}, \mathbf{r}_{\text{QE}}, \omega)$ .

### 3. Results and discussion

In this section, we present the results for the electromagnetic coupling between a quantum emitter and spherical metallic nanoantennas. First, in Section 3.1, we focus on the role of quantum phenomena by comparing quantum TDDFT and classical LRA results for a quantum emitter in front of a single spherical nanoantenna. Then, in Section 3.2, we compare results of TDDFT and the semiclassical Feibelman model for the same system. In Section 3.3, we use the Feibelman model to analyze the origin of the observed quantum effects, and discuss the validity range and shortcomings of the long-wavelength Feibelman approach that neglects the nonlocality of the metal response in the direction parallel to the surface. Finally, in Section 3.4, we extend the present analysis to the case of a spherical dimer nanoantenna, showing that the surface quantum effects observed for the single spherical nanoparticle are also present in the dimer case and that the long-wavelength Feibelman model does not describe accurately situations of gap distances narrower than  $D \sim 1.5$  nm.

#### 3.1. Quantum TDDFT vs. classical LRA

We first analyze the quantum effects that influence the self-interaction Green’s function  $G(\mathbf{r}_{\text{QE}}, \mathbf{r}_{\text{QE}}, \omega)$  obtained for a QE placed in front of a single spherical nanoparticle. The QE is oriented in the radial direction perpendicular to the nanoparticle surface (see sketch in Fig. 1(a)). To identify the quantum effects, we first compare in Fig. 2 the classical LRA (panels a-b) and the TDDFT (c-d) results. We plot both the imaginary (a, c) and real (b, d) parts of  $G(\mathbf{r}_{\text{QE}}, \mathbf{r}_{\text{QE}}, \omega)$  determining the Purcell factor and Lamb shift, respectively. Results are shown as a function of the transition frequency of the QE,  $\omega$ , and the distance  $d$  between the QE and the surface of the spherical nanoparticle,  $d = R - a$ .

Classical LRA calculations predict a dependence of  $G(\mathbf{r}_{\text{QE}}, \mathbf{r}_{\text{QE}}, \omega)$  on frequency determined by various multipolar plasmon modes excited by the QE, resulting in several peaks in the spectra of  $\text{Im}\{G(\mathbf{r}_{\text{QE}}, \mathbf{r}_{\text{QE}}, \omega)\}$  (Fig. 2(a)). The three lower-frequency sharp resonances are associated with the dipolar (DP,  $\ell = 1$ ), quadrupolar (QP,  $\ell = 2$ ), and octupolar (OP,  $\ell = 3$ ) plasmons of the spherical nanoantenna. Their frequencies  $\omega_{\ell}$  are given by the poles of Eq. (16),

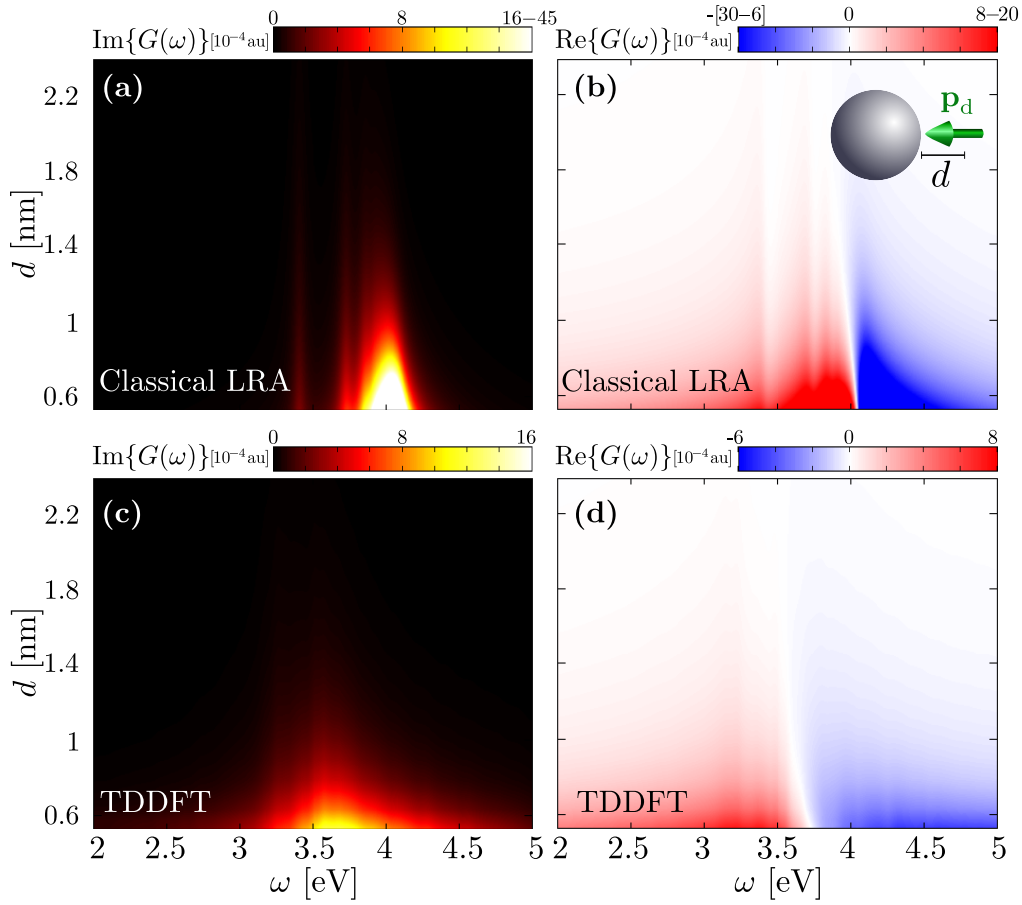


**Fig. 2.** (a,b) Classical LRA result of the (a) imaginary part ( $\text{Im}\{G(\mathbf{r}_{\text{QE}}, \mathbf{r}_{\text{QE}}, \omega)\}$ ), and (b) real part ( $\text{Re}\{G(\mathbf{r}_{\text{QE}}, \mathbf{r}_{\text{QE}}, \omega)\}$ ) of the self-interaction Green's function  $G(\mathbf{r}_{\text{QE}}, \mathbf{r}_{\text{QE}}, \omega)$  obtained for a point-like QE placed in front of a single Na spherical nanoantenna of radius  $a = 65.83 a_0$  ( $\approx 3.5$  nm). Results are shown as a function of the frequency  $\omega$  of the oscillating QE and the surface-to-emitter distance,  $d$ . Panels (c) and (d) correspond to the results obtained with TDDFT simulations. In (a) and (b), the upper and lower range of values in the color bar denote saturation.

$\text{Re}\left\{\epsilon_m(\omega_\ell) + \frac{\ell+1}{\ell}\right\} = 0$ , resulting for a metal described with a Drude dielectric function in

$$\omega_\ell = \omega_p \sqrt{\frac{\ell}{2\ell + 1}}. \quad (19)$$

From Eq. (19) it follows that the frequencies of the DP, QP and OP are respectively  $\omega_{\text{DP}} \approx 3.4$  eV,  $\omega_{\text{QP}} \approx 3.7$  eV, and  $\omega_{\text{OP}} \approx 3.85$  eV. The high-frequency broad peak at  $\omega_{\text{PSM}} \sim 4$  eV (i.e. close to the surface plasmon frequency  $\omega_{\text{SP}} = \omega_p/\sqrt{2}$ ) corresponds to the so-called *pseudomode* [127], which is composed by a piling up of several overlapping high-order plasmonic modes ( $\ell = 4, 5, 6, \dots$ ) with closely-spaced resonant frequencies.

At small  $d \approx 0.53 - 1$  nm,  $\text{Im}\{G(\mathbf{r}_{\text{QE}}, \mathbf{r}_{\text{QE}}, \omega)\}$ , as calculated within the classical LRA, is dominated by the pseudomode excitation. As the distance between the QE and the nanoantenna increases,  $\text{Im}\{G(\mathbf{r}_{\text{QE}}, \mathbf{r}_{\text{QE}}, \omega)\}$  decreases, and the relative contribution of different plasmon modes changes in favor of the low  $\ell$  resonances. Thus, for large  $d \sim 1.6 - 1.8$  nm, the values

of  $\text{Im}\{G(\mathbf{r}_{\text{QE}}, \mathbf{r}_{\text{QE}}, \omega)\}$  attained within the pseudomode frequency range become comparable to those at the sharp DP and QP resonances. The faster decrease of the resonances associated with high-order plasmon modes with increasing  $d$  can be inferred from Eq. (16), where  $R = a + d$ . We also note that the value of  $\text{Im}\{G(\mathbf{r}_{\text{QE}}, \mathbf{r}_{\text{QE}}, \omega)\}$  obtained for a QE resonant with the pseudomode at  $\omega_{\text{PSM}} = 4.05$  eV and located at  $d = 0.58$  nm corresponds to a Purcell factor  $F_p \approx 5.2 \times 10^6$  (Eq. (3)). This very large value is explained by the small volume of the nanoantenna (and thus strong field localization).

In contrast with the classical results,  $\text{Im}\{G(\mathbf{r}_{\text{QE}}, \mathbf{r}_{\text{QE}}, \omega)\}$  calculated with TDDFT (Fig. 2(c)) mainly reveals a single broad feature [128] for the range of distances considered in this study. At small separation  $d \approx 0.53 - 1$  nm, the maximum value of  $\text{Im}\{G(\mathbf{r}_{\text{QE}}, \mathbf{r}_{\text{QE}}, \omega)\}$  is reached within the frequency interval  $\omega \sim 3.6 - 3.7$  eV, i.e., it is redshifted with respect to the classical pseudomode peak. As  $d$  increases, the resonant feature slightly shifts to lower frequencies. Moreover, the overall profile somewhat sharpens, albeit, in sheer contrast with the classical theory, the contributions of different plasmon modes remain spectrally broader and are barely resolved. Consistent with the strong broadening of the plasmon resonances due to quantum effects, the TDDFT results show smaller values of  $\text{Im}\{G(\mathbf{r}_{\text{QE}}, \mathbf{r}_{\text{QE}}, \omega)\}$  at resonance, and thus lower QE decay rates, as compared to the classical LRA prediction. For example, for a QE placed at a distance  $d = 0.58$  nm, the resonant Purcell factor  $F_p$  calculated within TDDFT is  $F_p \approx 1.5 \times 10^6$ . This is more than three times smaller than the maximum LRA value. On the other hand, the broadening of the spectra leads to a larger off-resonant  $\text{Im}\{G(\mathbf{r}_{\text{QE}}, \mathbf{r}_{\text{QE}}, \omega)\}$  obtained with TDDFT as compared to classical LRA predictions.

We next compare the classical LRA and quantum TDDFT results for the real part of the self-interaction Green's function,  $\text{Re}\{G(\mathbf{r}_{\text{QE}}, \mathbf{r}_{\text{QE}}, \omega)\}$ , which determines the Lamb shift of the QE transition frequency. As depicted in Fig. 2(b), and consistent with the results obtained for the imaginary part of the Green's function (Fig. 2(a)), the frequency dependence of  $\text{Re}\{G(\mathbf{r}_{\text{QE}}, \mathbf{r}_{\text{QE}}, \omega)\}$  obtained from classical LRA calculations features a rich resonance profile. For an individual plasmonic mode, the Kramers-Kronig relations would lead to a sign change of  $\text{Re}\{G(\mathbf{r}_{\text{QE}}, \mathbf{r}_{\text{QE}}, \omega)\}$  at the resonance frequency. In the full calculations,  $\text{Re}\{G(\mathbf{r}_{\text{QE}}, \mathbf{r}_{\text{QE}}, \omega)\}$  does not show the sign change at resonance for low  $\ell$  modes and small distances, because of the off-resonant contribution associated with neighboring plasmon modes with larger  $\ell$ . It is only at the pseudomode frequency that the contribution of the nearly degenerate resonances leads to a change of sign of  $\text{Re}\{G(\mathbf{r}_{\text{QE}}, \mathbf{r}_{\text{QE}}, \omega)\}$  from positive values at frequencies below  $\omega_{\text{PSM}} \sim 4$  eV to negative values above this frequency. When  $d$  increases, the contribution from off-resonant neighboring modes is reduced so that, in addition to the pseudomode resonance, the sign change of  $\text{Re}\{G(\mathbf{r}_{\text{QE}}, \mathbf{r}_{\text{QE}}, \omega)\}$  can be observed at the DP and QP resonances. This appears particularly clear in Fig. 3 discussed below, where we show the frequency dependence of the Green's function calculated for a set of fixed separations,  $d$ , between the QE and the metallic surface.

As compared to the classical LRA, and similar to the results obtained for the imaginary part, the TDDFT calculations in Fig. 2(d) show smaller absolute values of  $\text{Re}\{G(\mathbf{r}_{\text{QE}}, \mathbf{r}_{\text{QE}}, \omega)\}$  (Lamb shift) and a broader structure at the resonant frequency  $\omega \sim 3.3 - 3.7$  eV. This holds for the entire distance  $d$  range considered in our study. Notably, a single broad resonance is formed in the TDDFT results and  $\text{Re}\{G(\mathbf{r}_{\text{QE}}, \mathbf{r}_{\text{QE}}, \omega)\}$  changes its sign from positive to negative only at the resonant frequency  $\omega \sim 3.3 - 3.7$  eV, i.e. at lower frequency than within the classical LRA. As a consequence, for QEs with transition frequencies within the range of  $\omega \sim 3.7 - 4$  eV, each model predicts a photonic Lamb shift  $\Delta\omega \propto \text{Re}\{G(\mathbf{r}_{\text{QE}}, \mathbf{r}_{\text{QE}}, \omega)\}$  of opposite sign (Eq. (2b)). For example, according to LRA, a QE located at  $d = 0.52$  nm and characterized by a transition dipole moment  $\mu = 0.1 e$  nm and vacuum resonant frequency  $\omega = 4$  eV experiences a redshift of  $\Delta\omega \approx -131$  meV. In contrast, TDDFT predicts a blueshift of  $\Delta\omega \approx 33$  meV under the same conditions.

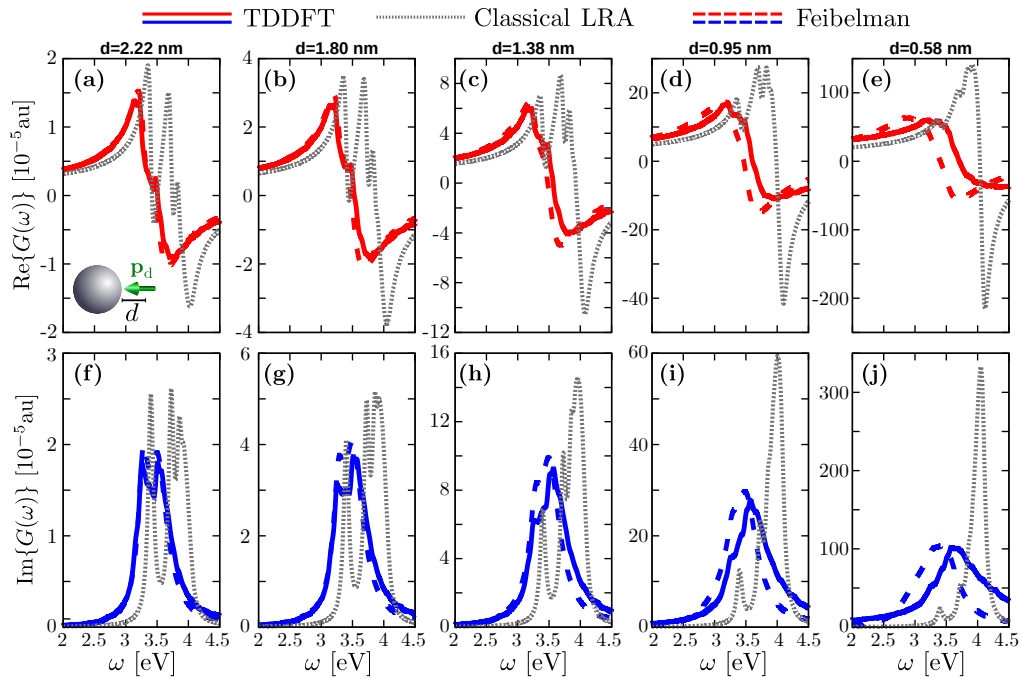


**Fig. 3.** Real part (upper panels a-e) and imaginary part (lower panels f-j) of the self-interaction Green's function obtained for a point-like dipole in front of a single spherical Na nanoantenna of radius  $a = 65.83 a_0 (\approx 3.5 \text{ nm})$ , as calculated from TDDFT (solid lines), within the Feibelman formalism (dashed lines) and within the classical LRA (dotted gray lines). Each panel corresponds to a selected surface-to-emitter distance  $d$ , ranging from  $d = 0.58 \text{ nm}$  (rightmost panels) to  $d = 2.22 \text{ nm}$  (leftmost panels), according to the labels on top.

### 3.2. Quantum TDDFT vs. semiclassical Feibelman approach

The semiclassical Feibelman formalism described in Section 2.3 is designed to account for quantum effects such as the nonlocality of the electron response and the spill-out of the induced charges that can be behind the differences between the classical LRA and TDDFT results discussed above. Analyzing the capability of the Feibelman formalism to reproduce the TDDFT results will thus allow for dissecting the role of these quantum effects in determining the plasmon resonances and their contribution to  $G(\mathbf{r}_{\text{QE}}, \mathbf{r}_{\text{QE}}, \omega)$ . To this end, we compare in Fig. 3 the real part (upper panels a-e) and the imaginary part (lower panels f-j) of  $G(\mathbf{r}_{\text{QE}}, \mathbf{r}_{\text{QE}}, \omega)$  as calculated using the three different approaches (TDDFT, LRA, and Feibelman). Results are shown as a function of the transition frequency of the QE, for selected values of the surface-to-emitter distance  $d$ . The solid and dashed color lines show the reference TDDFT results and the data obtained using the long-wavelength Feibelman formalism, respectively. The LRA results are plotted by gray-dotted lines. The overall good agreement between the TDDFT and the Feibelman formalism in Fig. 3 establishes the validity of the latter and allows us to use the framework of the Feibelman theory to analyze the role of the quantum phenomena manifested in  $G(\mathbf{r}_{\text{QE}}, \mathbf{r}_{\text{QE}}, \omega)$ , as we discuss below.

We first focus on the results at relatively large distance  $d = 1.38 - 2.22 \text{ nm}$  (panels a-c and f-h), where the agreement between the long-wavelength Feibelman approach and TDDFT is particularly good. The semiclassical Feibelman model accurately reproduces the TDDFT results of the spectral position and resonance profile of  $G(\mathbf{r}_{\text{QE}}, \mathbf{r}_{\text{QE}}, \omega)$ , thus correctly accounting for the

redshift and larger broadening of the peaks as compared to classical LRA. On the other hand, for distances below  $d \leq 0.95$  nm (panels d-e and i-j), the semiclassical Feibelman results are redshifted with respect to those of TDDFT, i.e., the semiclassical model overestimates the redshift of the plasmonic modes from the resonant frequencies obtained within the LRA as  $d$  decreases. Thus, based on this comparison, we conclude that for small QE–metal surface distances,  $d$ , the calculations based on the long-wavelength Feibelman parameters provide a qualitative agreement with TDDFT, but not quantitative accuracy.

### 3.3. Interpretation of the quantum effects within the Feibelman approach and its limitations

Both the overall good agreement and the discrepancy for small separation can be easily understood from the analytical Feibelman expression of  $G(\mathbf{r}_{\text{QE}}, \mathbf{r}_{\text{QE}}, \omega)$ . The resonant frequencies  $\omega_\ell$  can be found from the poles of Eq. (18),

$$\text{Re} \left\{ \varepsilon_m(\omega_\ell) + \frac{\ell + 1}{\ell} - (\varepsilon_m(\omega_\ell) - 1) \frac{\ell + 1}{a} d_\perp(\omega_\ell) \right\} = 0, \quad (20)$$

so that, for a Drude-type dielectric function (Eq. (15)),  $\omega_\ell$  can be obtained from the following expression:

$$\omega_\ell^2 \approx \omega_p^2 \frac{\ell}{2\ell + 1} \left( 1 - \underbrace{\frac{(\ell + 1)}{a} \text{Re} \{d_\perp(\omega_\ell)\}}_{\text{spill-out of the induced electron density}} \right), \quad (21)$$

where  $\omega_\ell \gg \gamma_p$  is assumed. Equation (21) shows similarities with expressions obtained within other nonlocal models [65]. For the present Na jellium material, where interband transitions are negligible, the finite electrostatic potential barrier at the jellium surface allows for the induced electron density to spill out of the metal boundary, giving rise to positive values of  $\text{Re} \{d_\perp(\omega)\}$  in the frequency range of interest [78]. The positive  $\text{Re} \{d_\perp(\omega)\}$  decreases  $\omega_\ell$  in Eq. (21) and we conclude that the spill-out of the induced electron density is responsible for the redshift of all the resonant frequencies  $\omega_\ell$ , as compared to the LRA values given by Eq. (19). This redshift is larger for plasmonic modes of higher order  $\ell$ .

To illustrate this discussion, we show in Fig. 4(a) the resonant frequencies  $\omega_\ell$  of the first ten plasmonic modes ( $\ell = 1 - 10$ ) of the single spherical nanoantenna as obtained from the LRA (Eq. (19), red dots), the TDDFT (orange dots) and the long-wavelength Feibelman model (Eq. (21), blue dots). For simplicity, we calculate the Feibelman  $\omega_\ell$  values as the frequency at which the imaginary part of the corresponding  $\ell$ -contribution to  $G(\mathbf{r}_{\text{QE}}, \mathbf{r}_{\text{QE}}, \omega)$ ,  $G_\ell(\mathbf{r}_{\text{QE}}, \mathbf{r}_{\text{QE}}, \omega)$ , is maximum (Eq. (18)), and we have checked that the results are consistent with Eq. (21). In Appendix C, we explain the procedure used to obtain the TDDFT values of  $\omega_\ell$ .

The results in Fig. 4(a) show good agreement between the TDDFT and the Feibelman formalism for the first four resonant frequencies  $\omega_\ell$  ( $\ell \leq 4$ ), which explains the match in the spectral position of  $G(\mathbf{r}_{\text{QE}}, \mathbf{r}_{\text{QE}}, \omega)$  obtained by the two models for relatively large distance  $d = 1.38 - 2.22$  nm, where the response is mostly dominated by these low-order modes (panels a-c and f-h of Fig. 3). However, for higher-order plasmonic modes  $\ell \gtrsim 5$ , the values of  $\omega_\ell$  within the semiclassical Feibelman formalism start to decrease with increasing  $\ell$ , instead of getting larger as occurs for small  $\ell$  and for the TDDFT results. Thus, the Feibelman approach results in considerably lower values of  $\omega_\ell$  as compared to the TDDFT predictions. As a consequence, since the relative contribution of these high-order modes  $\ell \gtrsim 5$  becomes important only for very small  $d$ , the Feibelman calculations produce an additional redshift of  $G(\mathbf{r}_{\text{QE}}, \mathbf{r}_{\text{QE}}, \omega)$  as compared to TDDFT for small separation distances  $d \leq 0.95$  nm. This effect can be clearly identified in panels d-e and i-j of Fig. 3. We believe that the mismatch between the Feibelman and the TDDFT values

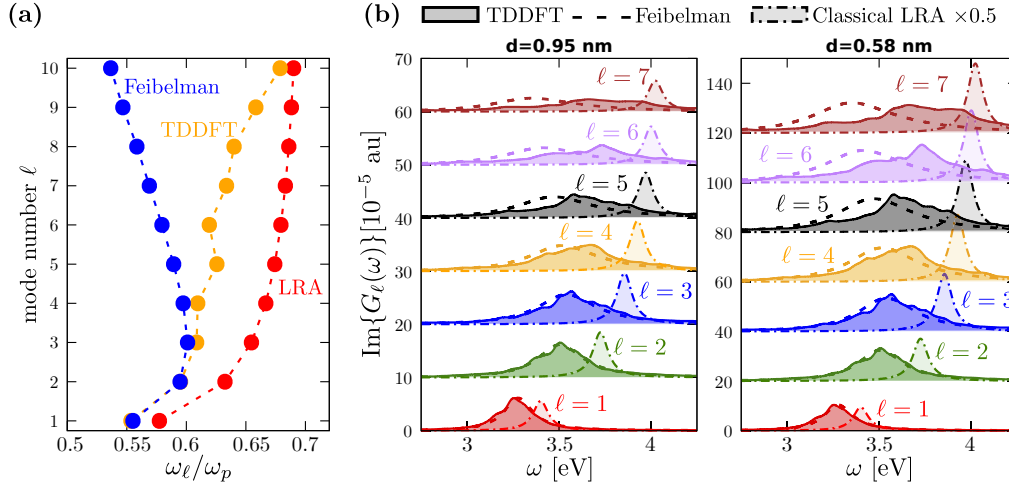


**Fig. 4.** (a) Resonant energies  $\omega_\ell$  of the first ten plasmonic modes ( $\ell = 1 - 10$ ) as obtained from the LRA (red dots), TDDFT (orange) and Feibelman model (blue), measured in units of the plasma frequency  $\omega_p = 5.89$  eV. (b) Contribution of the first seven plasmonic modes  $G_\ell(\mathbf{r}_{\text{QE}}, \mathbf{r}_{\text{QE}}, \omega)$  ( $\ell = 1 - 7$ ) to the imaginary part of the self-interaction Green's function  $G(\mathbf{r}_{\text{QE}}, \mathbf{r}_{\text{QE}}, \omega)$ , as obtained from TDDFT calculations (solid lines), within the Feibelman formalism (dashed lines) and within the classical LRA (dashed-dotted lines). Left-side panel corresponds to a surface-to-emitter distance  $d = 0.95$  nm, and right-side panel to  $d = 0.58$  nm. The spectra in panel (b) are shifted vertically for visibility.

of  $\omega_\ell$  for  $\ell \gtrsim 5$  is a consequence of the approximation adopted to implement the calculation of  $d_\perp(\omega)$ . Indeed, the  $d_\perp(\omega)$  parameter is obtained by considering the long-wavelength limit (small wavenumber in the direction parallel to the surface) [74] in a planar metal–vacuum interface [55,78], which translates, in the case of a spherical nanoparticle, into the condition  $\ell d_\perp(\omega)/a \ll 1$ . Thus, for a given radius  $a$  of a nanoparticle, large values of  $\ell$ , above a threshold value, do not fulfill this condition. Indeed, for small nanoantenna–QE separation, large  $\ell$  values are required, and thus the Feibelman approach under the long-wavelength limit becomes inaccurate in such a situation.

Additionally, the Feibelman formalism can also be used to explain the broad resonance profile of  $G(\mathbf{r}_{\text{QE}}, \mathbf{r}_{\text{QE}}, \omega)$  shown by the TDDFT results in Figs. 2 and 3. From Eq. (18), we infer that the broadening  $\kappa_\ell$  of the  $\ell$ -resonance,  $G_\ell(\mathbf{r}_{\text{QE}}, \mathbf{r}_{\text{QE}}, \omega)$ , is given within the Feibelman model by

$$\kappa_\ell \approx \gamma_p + \underbrace{\omega_\ell \frac{\ell + 1}{a} \text{Im}\{d_\perp(\omega_\ell)\}}_{\text{surface-enabled Landau damping}}, \quad (22)$$

which expresses an enhancement of the total damping  $\kappa_\ell$  produced by surface-enabled Landau damping because  $\text{Im}\{d_\perp(\omega_\ell)\}$  is positive [55]. As a consequence, different plasmonic  $\ell$ -modes within TDDFT spectrally overlap, giving rise to the generally broad profile of the total  $G(\mathbf{r}_{\text{QE}}, \mathbf{r}_{\text{QE}}, \omega)$ , which includes the contributions  $G_\ell(\mathbf{r}_{\text{QE}}, \mathbf{r}_{\text{QE}}, \omega)$  from all  $\ell$ -modes (Figs. 2 and 3) [128].

In order to illustrate the consequences of surface-enabled Landau damping, in Fig. 4(b) we show the contribution of the first seven plasmonic modes  $G_\ell(\mathbf{r}_{\text{QE}}, \mathbf{r}_{\text{QE}}, \omega)$  ( $\ell = 1 - 7$ ) to the spectra of the imaginary part of the self-interaction Green's function  $G(\mathbf{r}_{\text{QE}}, \mathbf{r}_{\text{QE}}, \omega)$ , as obtained from the three different models employed in this work. Results are shown for  $d = 0.95$  nm (left-side panel in b) and  $d = 0.58$  nm (right-side panel in b). As expected, within the classical



LRA (dashed-dotted lines) all the multipoles have the same broadening, with full width at half maximum (FWHM) equal to  $\gamma_p$ . In contrast, both TDDFT (solid lines) and the Feibelman model (dashed lines) predict an increasing of the FWHM with increasing plasmonic order  $\ell$ , as given by Eq. (22). Finally, the comparison of the results obtained for  $d = 0.95$  nm and  $d = 0.58$  nm, Fig. 4(b) corroborates that the relative contribution of higher-order plasmonic resonances increases with decreasing surface-to-emitter distance  $d$  within the three models employed in this work (LRA, TDDFT and Feibelman).

### 3.4. Quantum TDDFT vs. semiclassical Feibelman approach in a nanoparticle dimer

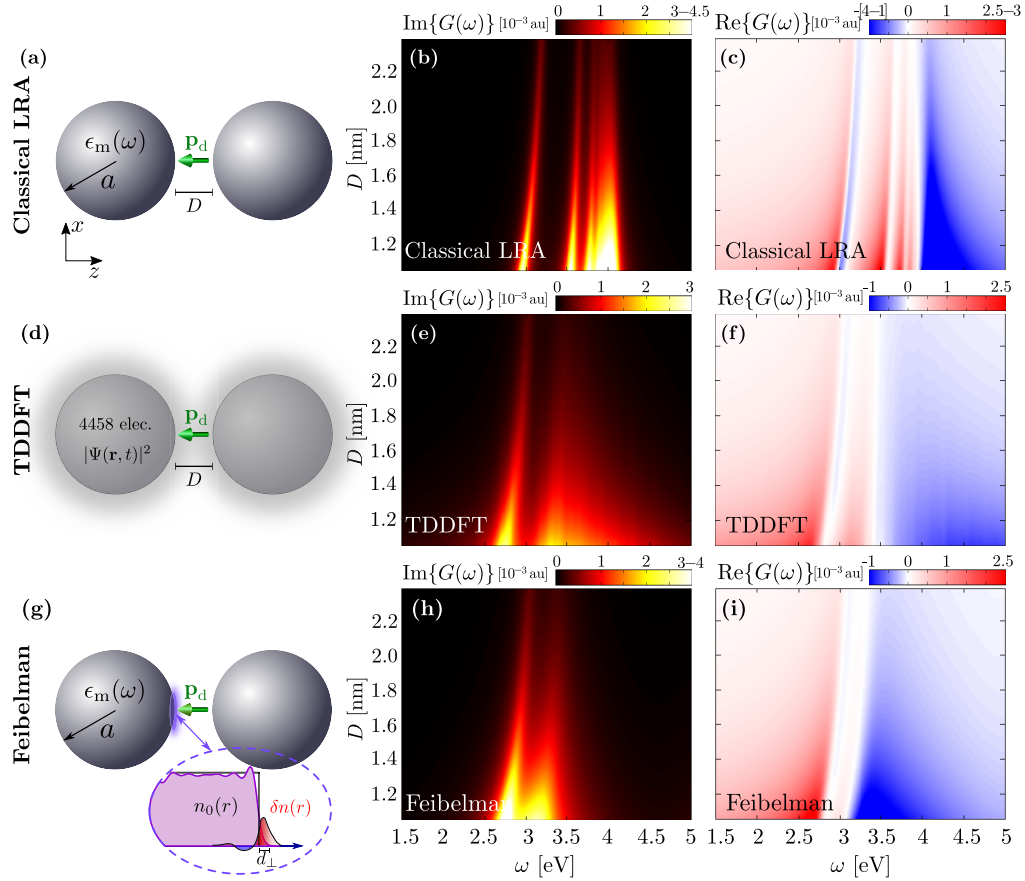
In this subsection, we extend the analysis to a metallic dimer nanoantenna comprising two identical spherical nanoparticles, where the QE is placed at the center of the gap of size  $D$ , as sketched in Fig. 1(b). This configuration has received special attention due to its capability to strongly enhance the amplitude of the incident electric field within the nanogap [129], leading to very efficient nanoantenna–QE interaction. Thus, the study of nonclassical effects in the dimer nanoantenna–QE coupling appears particularly interesting.

Figure 5 shows the real (right-side panels) and imaginary (center panels) parts of the self-interaction Green's function  $G(\mathbf{r}_{\text{QE}}, \mathbf{r}_{\text{QE}}, \omega)$  calculated for the dimer configuration, as provided by classical LRA calculations (top), TDDFT (middle), and the semiclassical Feibelman model (bottom). The QE is oriented along the dimer axis (the  $z$ -axis). Results are shown as a function of the transition frequency of the QE,  $\omega$ , and the size of the gap,  $D$ . Thus, the distance  $d$  between the QE and the surface of each nanoparticle forming the nanogap is  $d = D/2$ .

Both the imaginary part (Fig. 5(b)) and real part (Fig. 5(c)) of  $G(\mathbf{r}_{\text{QE}}, \mathbf{r}_{\text{QE}}, \omega)$  calculated within the classical LRA show similar behavior for the dimer configuration as for the single nanoantenna (compare Figs. 5(b-c) and 2(a-b)). For the range of the gap size  $D = 20 - 45 a_0$  ( $\approx 1.06 - 2.4$  nm) covered in Fig. 5, the classical LRA results show a rich resonance profile with at least three well-defined resonances, namely the bonding dipolar plasmon (BDP,  $\omega_{\text{BDP}} \sim 3$  eV), the bonding quadrupolar plasmon (BQP,  $\omega_{\text{BQP}} \sim 3.5$  eV) and the broad dimer pseudomode ( $\omega_{\text{PSM}} \sim 3.75 - 4.1$  eV). These BDP, BQP and pseudomode are formed due to the optical hybridization between the plasmonic  $\ell$ -order modes of the single nanoparticles [130]. For all the  $D$  values considered, the BDP and BQP resonances are narrow, while the pseudomode is broad because this mode originates from the hybridization of high-order plasmonic modes  $\ell \geq 3$  of the isolated nanoparticles with closely-spaced resonant frequency. The spectral weight of the pseudomode within the classical LRA considerably increases for small gap separations, and it becomes dominant for gaps smaller than  $D \lesssim 36 a_0$  ( $D \lesssim 1.9$  nm).

In contrast to these classical LRA predictions, the TDDFT results (panels e,f) show only two distinct modes: a BDP at  $\omega_{\text{BDP}} \sim 2.75$  eV and a pseudomode at  $\omega_{\text{PSM}} \sim 3.25 - 3.5$  eV. Within TDDFT, the BDP is the dominant resonance for the whole range of gap sizes covered in this work, and its spectral weight increases as the gap separation  $D$  becomes larger. The semiclassical Feibelman model (panels h-i in Fig. 5) accurately reproduces the TDDFT spectra when comparing the strength and the spectral position of the BDP and the pseudomode. The broadening of the BDP resonance is also well reproduced by the Feibelman model. However, we note that the pseudomode obtained from the Feibelman calculations is sharper (albeit still broad) than the one obtained within TDDFT. This effect is directly related to the redshift of the high-order modes  $\ell \gtrsim 5$  with increasing  $\ell$  shown by the Feibelman model in Fig. 4 for a single nanoantenna, which is expected to be reflected also in the dimer results. Since the high- $\ell$  resonances of the single nanoantenna have lower frequency, they cannot contribute to the broadening of the pseudomode in the large frequency range  $\omega_{\text{PSM}} \sim 3.5$  eV.

For the sake of a quantitative comparison between the LRA, TDDFT and Feibelman results, we show in Fig. 6 the frequency dependence of  $G(\mathbf{r}_{\text{QE}}, \mathbf{r}_{\text{QE}}, \omega)$  calculated for a set of fixed gap separations  $D$ , as obtained from a cut of Fig. 5. Although there are quantitative discrepancies



**Fig. 5.** Self-interaction Green's function  $G(\mathbf{r}_{\text{QE}}, \mathbf{r}_{\text{QE}}, \omega)$  obtained for a point-like QE placed at the center of the gap of size  $D$  formed by two identical Na spherical nanoantennas of radius  $a = 65.83 a_0 (\approx 3.5 \text{ nm})$ . The QE is oriented along the dimer  $z$ -axis. **a-d-g** Sketches of the system studied within the three models employed in this work: **(a)** classical LRA, where the dielectric response of the metal is described by a local dielectric function  $\epsilon_m(\omega)$  and standard hard-wall boundary conditions are applied at the metal–vacuum interface, **(d)** TDDFT, where the time evolution of the electron density  $n(\mathbf{r}, t) = \sum_{j \in \text{occ}} \chi_j |\Psi_j(\mathbf{r}, t)|^2$  is obtained from the time-dependent KS equations and **(g)** Feibelman model, which uses the local dielectric function  $\epsilon_m(\omega)$  to describe the bulk response of the metals but incorporates quantum surface-response corrections at the metal–vacuum interface by means of the  $d_{\perp}(\omega)$  parameter. Imaginary part (panels **b-e-h**) and real part (**c-f-i**) of the self-interaction Green's function  $G(\mathbf{r}_{\text{QE}}, \mathbf{r}_{\text{QE}}, \omega)$  as obtained from the classical LRA (**b-c**), TDDFT (**e-f**) and Feibelman model (**h-i**). Results are shown as a function of the transition frequency of the QE,  $\omega$ , and the size of the gap,  $D$ . In **(b)**, **(c)**, and **(h)**, the upper and lower range of values in the colorbar denote saturation.

between the TDDFT and the Feibelman results for narrow gaps  $D \sim 1 - 1.5$  nm (panels d, e, i, j in Fig. 6), the overall good agreement between the two approaches indicates that the spill-out of the induced charges and surface-enabled Landau damping, already discussed in the single-nanoantenna system, are also the main quantum mechanisms influencing  $G(\mathbf{r}_{\text{QE}}, \mathbf{r}_{\text{QE}}, \omega)$  in the dimer nanoantenna. Moreover, these results corroborate the validity of the long-wavelength limit implementation of the Feibelman approach to adequately describe the electromagnetic interaction between a QE and a plasmonic gap nanoantenna for situations where the gap separation is larger than  $D \sim 1.5$  nm (panels a, b, c, f, g, h in Fig. 6). However, similar to the single-nanoparticle case in Sections 3.2 and 3.3, for smaller gap separations in a dimer,  $D < 1.5$  nm, the limitations of the approximation used to obtain the Feibelman parameter (neglecting the dependence of  $d_{\perp}(\omega)$  on the wavenumber parallel to the metal surface) affects the accuracy of the results, since in such a case, high-order plasmonic modes  $\ell$  are also relevant.

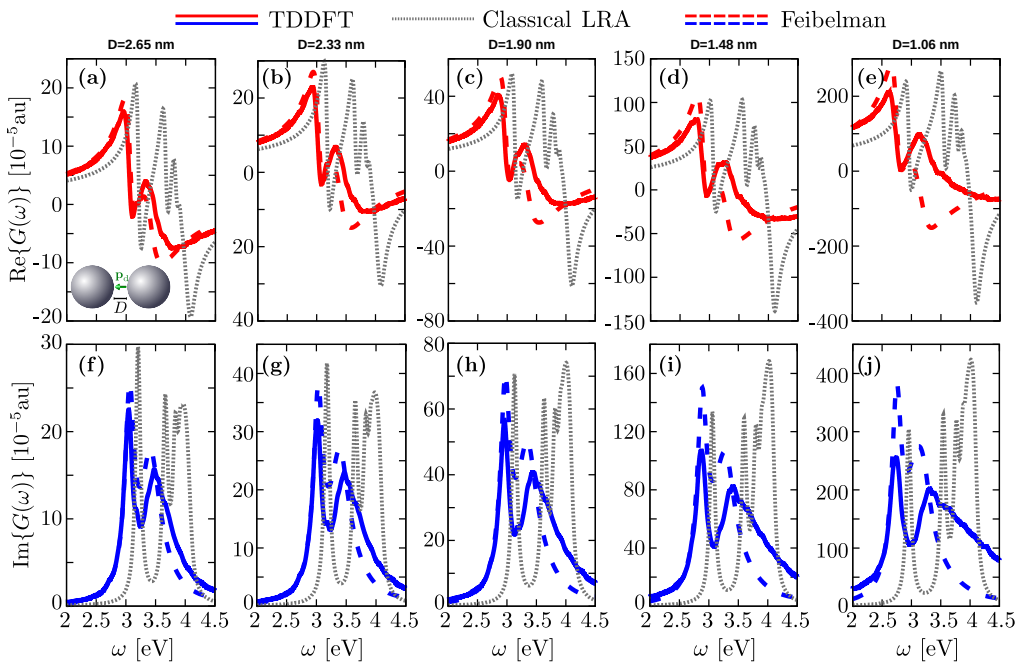


**Fig. 6.** Real part (upper panels a-e) and imaginary part (lower panels f-j) of the self-interaction Green's function obtained for a point-like dipole placed at the center of a gap of size  $D$  formed by two identical Na spherical nanoantennas of radius  $a = 65.83 a_0 (\approx 3.49$  nm), as calculated from TDDFT (solid lines), within the Feibelman formalism (dashed lines) and within the classical LRA (dotted gray lines). Each panel corresponds to selected gap sizes  $D$  ranging from  $D = 1.06$  nm (rightmost panels) to  $D = 2.65$  nm (leftmost panels). Gap separation distances are indicated on the top panels.

#### 4. Summary and conclusions

In this work, we study the influence of quantum phenomena on the electromagnetic interaction between a point-like quantum emitter (QE) and canonical metallic nanoantennas. We focus on the study of the self-interaction dyadic Green's function  $\hat{G}(\mathbf{r}_{\text{QE}}, \mathbf{r}_{\text{QE}}, \omega)$  obtained for a single spherical nanoparticle and a dimer comprising two identical spherical nanoparticles, with the QE oriented perpendicular to the metal surfaces. In the case of the dimer, the QE is located

in the middle of the gap. We consider sufficiently large nanoantenna–QE separations so that charge-transfer processes related to electron tunneling do not play a role.

We first calculate  $\hat{G}(\mathbf{r}_{\text{QE}}, \mathbf{r}_{\text{QE}}, \omega)$  in the presence of Na jellium nanoparticles using time-dependent density functional theory (TDDFT), and then employ analytical expressions derived from a semiclassical model in order to identify the origin of the quantum effects that influence the nanoantenna–QE coupling. This semiclassical model incorporates surface quantum-response corrections by means of the Feibelman  $d_{\perp}(\omega)$  parameter obtained under the long-wavelength limit. The overall good agreement between TDDFT and the semiclassical model for both the single and the dimer antennas confirms that surface-enabled Landau damping and the spill-out of the induced electron density drastically affect the electromagnetic nanoantenna–QE interaction. These mechanisms explain why the resonances of  $\hat{G}(\mathbf{r}_{\text{QE}}, \mathbf{r}_{\text{QE}}, \omega)$  obtained from TDDFT are redshifted and broader as compared to those obtained from a classical calculation using the local-response approximation (LRA) of the optical response of the metals.

We find that these quantum effects become more significant with increasing order  $\ell$  of the plasmonic resonance. The analysis of the TDDFT calculations indicates that the higher the value of  $\ell$ , the larger the broadening  $\kappa_{\ell}$  produced by surface-enabled Landau damping and the redshift produced by the spill-out of the dynamical screening charges. Thus, the quantum phenomena explored here show greater influence for very small distance between the QE and the metallic surface and when the QE is coupled to high-order plasmonic modes of the nanoantenna.

We also find that the long-wavelength Feibelman calculations employed in this work describe more accurately the Green's function of a dipolar emitter when considering QEs coupled to low-order plasmonic modes. However, these calculations fail when the contribution from antenna high-order modes ( $\ell \gtrsim 5$ ) is large, as occurs when the distance  $d$  between the QE and the nanoantenna is very small,  $d \sim 0.6$  nm. As a consequence, in the dimer configuration the present Feibelman calculations underestimate the broadening of the pseudomode and become inaccurate for gap separations of the order of  $D \sim 1 - 1.5$  nm.

The shortcomings of the Feibelman calculations are due to the limitations of using a  $d_{\perp}(\omega)$  parameter obtained for a model planar metal–vacuum interface where the dependence of  $d_{\perp}(\omega)$  on the wavenumber parallel to the metal surface (or, equivalently, angular momentum  $\ell$  for spherical nanoparticles) is neglected. For more accurate results, it is necessary to go beyond this long-wavelength limit of  $d_{\perp}(\omega)$  to properly account for the nonlocality of the surface response in the direction parallel to the surface, since this affects the results in situations where the nanoantenna–QE distance is small (high-order  $\ell$  modes involved).

Our study thus provides a fundamental description of the quantum phenomena influencing the electromagnetic interaction between a QE and plasmonic nanoantennas for nanoantenna–QE distances as small as  $\approx 0.5$  nm. For even smaller separation, charge-transfer processes between the QE and the metallic nanoantenna can influence the optoelectronic response of the system, so that a many-body treatment based on TDDFT of both the QE and the metallic nanoparticles [38] is well suited to naturally account for any quantum effect in these extreme situations.

## Appendices

### A. Determining the damping parameter $\gamma_p$ used in the LRA and in the Feibelman calculations

The value of the damping parameter  $\gamma_p$  used in the Drude-type dielectric function  $\epsilon_m(\omega)$  (Eq. (15)) for the classical LRA and in the Feibelman results is obtained from the fitting of the absorption cross-section spectrum  $\sigma_{\text{abs}}(\omega)$  of a single Na nanoparticle calculated with TDDFT to the result obtained within the Feibelman model. The absorption cross section  $\sigma_{\text{abs}}(\omega)$  reads

$$\sigma_{\text{abs}}(\omega) = \frac{4\pi\omega}{c} \text{Im}\{\alpha(\omega)\}, \quad (23)$$

where  $c$  is the speed of light and  $\alpha(\omega)$  the polarizability of the spherical particle of radius  $a$ . Within the Feibelman formalism (for  $d_{\parallel}(\omega) = 0$ ),  $\alpha(\omega)$  is given by

$$\alpha(\omega) = a^3 \frac{(\epsilon_m(\omega) - 1)(1 + d_{\perp}(\omega)/a)}{\epsilon_m(\omega) + 2 - 2(\epsilon_m(\omega) - 1)d_{\perp}(\omega)/a}, \quad (24)$$

with  $a = 65.83 a_0$  the radius of the single spherical nanoparticle. The polarizability within the TDDFT is obtained from the dipole moment induced in response to an impulsive plane-wave excitation, as explained in Ref. [117]. Figure 7 shows very good agreement between the TDDFT results (solid blue line) and the Feibelman formalism (dashed red line) when using  $\gamma_p = 0.1$  eV, thus justifying the value used in this work.

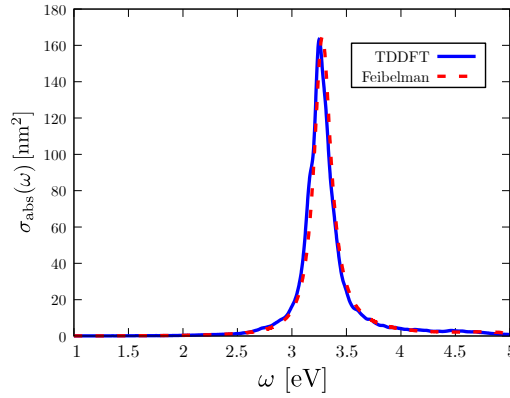


**Fig. 7.** Comparison between the absorption cross section obtained from TDDFT calculations (solid blue line) and within the Feibelman formalism using an intrinsic damping parameter  $\gamma_p = 0.1$  eV in the Drude dielectric function given by Eq. (15) (dashed red line). The spherical nanoparticle contains 4458 conduction electrons, resulting in a radius of  $a = 65.83 a_0$ .

## B. Introducing the Feibelman $d_{\perp}(\omega)$ parameter in the optical response of a spherical dimer

The self-interaction Green's function  $G(\mathbf{r}_{QE}, \mathbf{r}_{QE}, \omega)$  of a spherical dimer antenna is obtained within the Feibelman formalism from the potential  $V_{\text{ind}}(\mathbf{r}, \omega)$  (Eq. (13)) induced in response to the external potential  $V_{\text{ext}}(\mathbf{r})$  of a point dipole (Eq. (12)) by applying the modified boundary conditions given by Eq. (17). This induced potential can be written as a sum of the contributions of each nanoparticle forming the dimer,  $V_{\text{ind}}(\mathbf{r}_1, \omega) = V_{\text{ind},1}(\mathbf{r}_1, \omega) + V_{\text{ind},2}(\mathbf{r}_2, \omega)$ . The position vectors  $\mathbf{r}_1$  and  $\mathbf{r}_2$ , with origins at the center of the corresponding nanoparticle, are related in spherical coordinates  $[(r_i, \theta_i, \varphi_i)]$  with  $i = 1, 2$ ] by  $r_2 = \sqrt{r_1^2 + (2a + D)^2 - 2(2a + D)r_1 \cos \theta_1}$ ,  $\cos \theta_2 = (r_1 \cos \theta_1 - (2a + D))/r_2$ , and  $\varphi_2 = \varphi_1$ .

Due to the spherical symmetry of the nanoparticles, it is convenient to expand  $V_{\text{ind},i}(\mathbf{r}_i, \omega)$  (with  $i = 1, 2$ ) inside ( $r_i < a$ ) and outside ( $r_i > a$ ) the metal boundaries in a spherical harmonics basis set  $Y_{\ell}^m(\theta_i, \varphi_i)$  [125],

$$V_{\text{ind},i}(\mathbf{r}_1, \omega) = \sum_{\ell=0}^{\ell_{\text{max}}} \sum_{m=-\ell}^{\ell} b_i^{\ell m}(\omega) Y_{\ell}^m(\theta_i, \varphi_i) \begin{cases} r_i^{\ell}/a^{\ell} & r_i < a \\ a^{\ell+1}/r_i^{\ell+1} & r_i > a, \end{cases}, \quad (25)$$

where  $\ell_{\text{max}}$  is an integer number large enough to achieve convergence.

The coefficients  $b_i^{\ell m}(\omega)$  (with  $i = 1, 2$ ) are determined by applying the modified boundary conditions given by Eq. (17). For  $d_{\parallel}(\omega) = 0$ , we obtain

$$\begin{aligned} b_1^{\ell m}(\omega) &= \xi(a, \ell, \omega) \int_{\Omega_1} d\Omega_1 [Y_{\ell}^m(\theta_1, \varphi_1)]^* \frac{\partial}{\partial r_1} (V_{\text{ext}}(\mathbf{r}_1) + V_{\text{ind},2}(\mathbf{r}_2, \omega)) \Big|_{r_1=a}, \\ b_2^{\ell m}(\omega) &= \xi(a, \ell, \omega) \int_{\Omega_2} d\Omega_2 [Y_{\ell}^m(\theta_2, \varphi_2)]^* \frac{\partial}{\partial r_2} (V_{\text{ext}}(\mathbf{r}_2) + V_{\text{ind},1}(\mathbf{r}_1, \omega)) \Big|_{r_2=a}, \end{aligned} \quad (26)$$

with

$$\xi(a, \ell, \omega) = \frac{-a(\varepsilon_m(\omega) - 1)(1 + \ell d_{\perp}(\omega)/a)}{(\ell + 1)(1 + \ell d_{\perp}(\omega)/a) + \ell \varepsilon_m(\omega)(1 - (\ell + 1)d_{\perp}(\omega)/a)}, \quad (27)$$

and the integrals extending over the solid angles  $\Omega_i = \{\theta_i, \phi_i\}$ .

Inserting Eq. (25) into Eq. (26), the coefficients  $b_1^{\ell m}(\omega)$  and  $b_2^{\ell m}(\omega)$  can be written in matrix form,

$$\begin{aligned} b_1^{\ell m}(\omega) &= \left( \mathbb{I} - \mathbb{T}^{2 \rightarrow 1} \mathbb{T}^{1 \rightarrow 2} \right)^{-1} \left( b_{\text{ext},1}^{\ell m}(\omega) + \mathbb{T}^{2 \rightarrow 1} b_{\text{ext},2}^{\ell m}(\omega) \right), \\ b_2^{\ell m}(\omega) &= \left( \mathbb{I} - \mathbb{T}^{1 \rightarrow 2} \mathbb{T}^{2 \rightarrow 1} \right)^{-1} \left( b_{\text{ext},2}^{\ell m}(\omega) + \mathbb{T}^{1 \rightarrow 2} b_{\text{ext},1}^{\ell m}(\omega) \right), \end{aligned} \quad (28)$$

where  $\mathbb{I}$  is the identity matrix,

$$b_{\text{ext},i}^{\ell m}(\omega) = \xi(a, \ell, \omega) \int_{\Omega_i} d\Omega_i [Y_{\ell}^m(\theta_i, \varphi_i)]^* \frac{\partial}{\partial r_i} V_{\text{ext}}(\mathbf{r}_i) \Big|_{r_i=a}, \quad (29)$$

and the elements  $(\ell m, \ell' m')$  of matrices  $\mathbb{T}^{2 \rightarrow 1}$  and  $\mathbb{T}^{1 \rightarrow 2}$  are given by

$$\begin{aligned} \mathbb{T}_{\ell m, \ell' m'}^{2 \rightarrow 1} &= \xi(a, \ell, \omega) \int_{\Omega_1} d\Omega_1 [Y_{\ell}^m(\theta_1, \varphi_1)]^* \frac{\partial}{\partial r_1} \left( Y_{\ell'}^{m'}(\theta_2, \varphi_2) \frac{a^{\ell'+1}}{r_2^{\ell'+1}} \right) \Big|_{r_1=a}, \\ \mathbb{T}_{\ell m, \ell' m'}^{1 \rightarrow 2} &= \xi(a, \ell, \omega) \int_{\Omega_2} d\Omega_2 [Y_{\ell}^m(\theta_2, \varphi_2)]^* \frac{\partial}{\partial r_2} \left( Y_{\ell'}^{m'}(\theta_1, \varphi_1) \frac{a^{\ell'+1}}{r_1^{\ell'+1}} \right) \Big|_{r_2=a}. \end{aligned} \quad (30)$$

Once the coefficients  $b_1^{\ell m}(\omega)$  and  $b_2^{\ell m}(\omega)$  are obtained by solving Eq. (28), the electric potential induced by each metallic nanoparticle is completely determined according to Eq. (25), and therefore, the self-interaction Green's function of a spherical dimer within the Feibelman model can be straightforwardly calculated using  $G_{\text{F}}(\mathbf{r}_{\text{QE}}, \mathbf{r}_{\text{QE}}, \omega) = -\nabla V_{\text{ind}}(\mathbf{r} = \mathbf{r}_{\text{QE}}, \omega)$ . Notice that the same procedure reported in this Appendix is used to obtain the classical LRA results of the dimer, where one can apply the condition  $d_{\perp}(\omega) = 0$ , and thus  $\xi(a, \ell, \omega) = \frac{-a(\varepsilon_m(\omega) - 1)}{(\ell + 1) + \ell \varepsilon_m(\omega)}$ .

### C. Contribution of plasmonic modes of order $\ell$ to the total self-interaction Green's function within TDDFT

In this Appendix, we explain how we obtain within TDDFT the resonant frequencies  $\omega_{\ell}$  shown in Fig. 4(a), as well as the contribution  $G_{\ell}(\mathbf{r}_{\text{QE}}, \mathbf{r}_{\text{QE}}, \omega)$  of different plasmonic modes of order  $\ell$  to the total Green's function spectra shown in Fig. 4(b). The self-interaction Green's function  $G(\mathbf{r}_{\text{QE}}, \mathbf{r}_{\text{QE}}, \omega)$  of the studied metallic nanoantennas is obtained within TDDFT from the time-dependent Hartree potential  $V_{\text{h}}[n](\mathbf{r}, t)$  (Eq. (10)). This Hartree potential satisfies Poisson's equation

$$\nabla^2 V_{\text{h}}[n](\mathbf{r}, t) = -4\pi(n(\mathbf{r}, t) - n_+). \quad (31)$$

For the single spherical metallic nanoparticle subjected to external illumination polarized along the  $z$ -axis, the system possesses rotational symmetry with respect to the  $z$ -axis, i.e., it



is independent of the azimuth angle  $\varphi$ . It is thus convenient to write  $V_h[n](\mathbf{r}, t)$  as a sum of Legendre polynomials  $P_\ell(\cos \theta)$ ,

$$V_h[n](\mathbf{r}, t) = \sum_{\ell=0}^{\infty} \frac{1}{r} \phi_\ell(r) P_\ell(\cos \theta). \quad (32)$$

Then, by expressing the operator  $\nabla^2$  in spherical coordinates, Eq. (31) can be written as

$$\sum_{\ell=0}^{\infty} \frac{1}{r} \underbrace{\left[ \frac{d^2}{dr^2} - \frac{\ell(\ell+1)}{r^2} \right]}_{\mathbb{A}_\ell} \phi_\ell(r) P_\ell(\cos \theta) = -4\pi \sum_{\ell=0}^{\infty} n_\ell(r, t) P_\ell(\cos \theta), \quad (33)$$

where

$$n_\ell(r, t) = \frac{2}{2\ell+1} \int_{-1}^1 (n(\mathbf{r}, t) - n_+) P_\ell(\cos \theta) d(\cos \theta), \quad (34)$$

and we express the operator  $\mathbb{A}_\ell = \left[ \frac{d^2}{dr^2} - \frac{\ell(\ell+1)}{r^2} \right]$  in matrix form using the method of Fourier-Grid-Hamiltonian [131].

From Eq. (33),  $\phi_\ell(r, t)$  is then directly obtained from

$$\phi_\ell(r, t) = -4\pi \mathbb{A}_\ell^{-1} [r n_\ell(r, t)]. \quad (35)$$

Thus, according to Eqs. (10)–11 the contribution  $G_\ell(\mathbf{r}_{\text{QE}}, \mathbf{r}_{\text{QE}}, \omega)$  of the different plasmonic  $\ell$ -modes to the total self-interaction Green's function  $G(\mathbf{r}_{\text{QE}}, \mathbf{r}_{\text{QE}}, \omega)$  can be obtained within TDDFT from

$$G_\ell(\mathbf{r}_{\text{QE}}, \mathbf{r}_{\text{QE}}, \omega) = \frac{1}{p_d} \int_0^{T_F} \nabla \phi_\ell(r = r_{\text{QE}}, t) P_\ell(\cos \theta = 1) e^{i(\omega+i\eta/2)t} dt, \quad (36)$$

with  $T_F = 3500$  au the total propagation time and  $\eta = 0.07$  eV.

The TDDFT results of  $G_\ell(\mathbf{r}_{\text{QE}}, \mathbf{r}_{\text{QE}}, \omega)$  obtained from Eq. (36) do not follow a perfect Lorentzian profile (Fig. 4(b)), and therefore defining a resonant frequency  $\omega_\ell$  of the plasmonic mode  $\ell$  is not straightforward. This is particularly evident in the case of resonances with large plasmonic order  $\ell$ , which exhibit a broad and complex spectral structure. In this study, we define the resonant frequency  $\omega_\ell$  within TDDFT (shown in Fig. 4(a)) as the mean value between the two frequencies at which  $\text{Im}\{G_\ell(\mathbf{r}_{\text{QE}}, \mathbf{r}_{\text{QE}}, \omega)\}$  is half of the maximum value.

**Funding.** Villum Fonden (16498); Department of Education of the Basque Government (IT1164-19); MCIN/AEI/10.13039/501100011033/ (PID2019-107432GB-I00).

**Acknowledgments.** A. B thanks the hospitality and nice atmosphere at the Institut des Sciences Moléculaires d'Orsay, France, and also the Department of Education of the Basque Government for a predoctoral fellowship (Grant No. PRE2017\_1\_0267). N. A. M. is a VILLUM Investigator supported by VILLUM FONDEN (Grant No. 16498). P. E. S. is the recipient of the Zonta Denmark's Scholarship for female PhD students in Science and Technology 2021.

**Disclosures.** The authors declare no conflict of interest.

**Data availability.** Data underlying the results presented in this paper are not publicly available at this time but may be obtained from the authors upon reasonable request.

## References

1. L. Novotny and N. van Hulst, "Antennas for light," *Nat. Photonics* **5**(2), 83–90 (2011).
2. K. Santhosh, O. Bitton, L. Chuntanov, and G. Haran, "Vacuum Rabi splitting in a plasmonic cavity at the single quantum emitter limit," *Nat. Commun.* **7**(1), 11823 (2016).
3. D. Melnikau, R. Esteban, D. Savateeva, A. Sánchez-Iglesias, M. Grzelczak, M. K. Schmidt, L. M. Liz-Marzán, J. Aizpurua, and Y. P. Rakovich, "Rabi splitting in photoluminescence spectra of hybrid systems of gold nanorods and J-aggregates," *J. Phys. Chem. Lett.* **7**(2), 354–362 (2016).

4. T. B. Hoang, G. M. Akselrod, and M. H. Mikkelsen, "Ultrafast room-temperature single photon emission from quantum dots coupled to plasmonic nanocavities," *Nano Lett.* **16**(1), 270–275 (2016).
5. T. Wang and C. A. Nijhuis, "Molecular electronic plasmonics," *Appl. Mater. Today* **3**, 73–86 (2016).
6. W. Du, T. Wang, H.-S. Chu, and C. A. Nijhuis, "Highly efficient on-chip direct electronic–plasmonic transducers," *Nat. Photonics* **11**(10), 623–627 (2017).
7. M. Parzefall, Á. Szabó, T. Taniguchi, K. Watanabe, M. Luisier, and L. Novotny, "Light from van der Waals quantum tunneling devices," *Nat. Commun.* **10**(1), 292 (2019).
8. P. Törmä and W. L. Barnes, "Strong coupling between surface plasmon polaritons and emitters: a review," *Rep. Prog. Phys.* **78**, 013901 (2014).
9. R. Chikkaraddy, B. De Nijs, F. Benz, S. J. Barrow, O. A. Scherman, E. Rosta, A. Demetriadou, P. Fox, O. Hess, and J. J. Baumberg, "Single-molecule strong coupling at room temperature in plasmonic nanocavities," *Nature* **535**(7610), 127–130 (2016).
10. R. Liu, Z.-K. Zhou, Y.-C. Yu, T. Zhang, H. Wang, G. Liu, Y. Wei, H. Chen, and X.-H. Wang, "Strong light-matter interactions in single open plasmonic nanocavities at the quantum optics limit," *Phys. Rev. Lett.* **118**(23), 237401 (2017).
11. D. G. Baranov, M. Wersäll, J. Cuadra, T. J. Antosiewicz, and T. Shegai, "Novel nanostructures and materials for strong light–matter interactions," *ACS Photonics* **5**(1), 24–42 (2018).
12. H. Leng, B. Szychowski, M.-C. Daniel, and M. Pelton, "Strong coupling and induced transparency at room temperature with single quantum dots and gap plasmons," *Nat. Commun.* **9**(1), 4012 (2018).
13. A. F. Kockum, A. Miranowicz, S. De Liberato, S. Savasta, and F. Nori, "Ultrastrong coupling between light and matter," *Nat. Rev. Phys.* **1**(1), 19–40 (2019).
14. E. Fort and S. Grésillon, "Surface enhanced fluorescence," *J. Phys. D: Appl. Phys.* **41**(1), 013001 (2007).
15. J. R. Lakowicz, *Principles of fluorescence spectroscopy* (Springer science & business media, 2013).
16. S. N. Gupta, O. Bitton, T. Neuman, R. Esteban, L. Chuntunov, J. Aizpurua, and G. Haran, "Complex plasmon-exciton dynamics revealed through quantum dot light emission in a nanocavity," *Nat. Commun.* **12**(1), 1310 (2021).
17. J. V. Pellegrotti, E. Cortés, M. D. Bordenave, M. Caldarola, M. P. Kreuzer, A. D. Sanchez, I. Ojea, A. V. Bragas, and F. D. Stefani, "Plasmonic photothermal fluorescence modulation for homogeneous biosensing," *ACS Sens.* **1**(11), 1351–1357 (2016).
18. F. Madzharova, A. Nodar, V. Zivanovic, M. R. S. Huang, C. T. Koch, R. Esteban, J. Aizpurua, and J. Kneipp, "Gold- and silver-coated barium titanate nanocomposites as probes for two-photon multimodal microspectroscopy," *Adv. Funct. Mater.* **29**(49), 1904289 (2019).
19. B. Doppagne, T. Neuman, R. Soria-Martinez, L. E. P. López, H. Bulou, M. Romeo, S. Berciaud, F. Scheurer, J. Aizpurua, and G. Schull, "Single-molecule tautomerization tracking through space- and time-resolved fluorescence spectroscopy," *Nat. Nanotechnol.* **15**(3), 207–211 (2020).
20. B. Yang, G. Chen, A. Ghafoor, Y. Zhang, Y. Zhang, Y. Zhang, Y. Luo, J. Yang, V. Sandoghdar, J. Aizpurua, Z. Dong, and J. G. Hou, "Sub-nanometre resolution in single-molecule photoluminescence imaging," *Nat. Photonics* **14**(11), 693–699 (2020).
21. G. W. Ford and W. H. Weber, "Electromagnetic interactions of molecules with metal surfaces," *Phys. Rep.* **113**(4), 195–287 (1984).
22. E. Waks and D. Sridharan, "Cavity QED treatment of interactions between a metal nanoparticle and a dipole emitter," *Phys. Rev. A* **82**(4), 043845 (2010).
23. J. Galego, F. J. Garcia-Vidal, and J. Feist, "Cavity-induced modifications of molecular structure in the strong-coupling regime," *Phys. Rev. X* **5**(4), 041022 (2015).
24. Y.-J. Zhao, M. Tian, X.-Y. Wang, H. Yang, H. Zhao, and Y.-G. Huang, "Quasi-static method and finite element method for obtaining the modifications of the spontaneous emission rate and energy level shift near a plasmonic nanostructure," *Opt. Express* **26**(2), 1390–1401 (2018).
25. T. P. Rossi, T. Shegai, P. Erhart, and T. J. Antosiewicz, "Strong plasmon-molecule coupling at the nanoscale revealed by first-principles modeling," *Nat. Commun.* **10**(1), 3336 (2019).
26. R. Carminati, J.-J. Greffet, C. Henkel, and J.-M. Vigoureux, "Radiative and non-radiative decay of a single molecule close to a metallic nanoparticle," *Opt. Commun.* **261**(2), 368–375 (2006).
27. T. Neuman, C. Huck, J. Vogt, F. Neubrech, R. Hillenbrand, J. Aizpurua, and A. Pucci, "Importance of plasmonic scattering for an optimal enhancement of vibrational absorption in seira with linear metallic antennas," *J. Phys. Chem. C* **119**(47), 26652–26662 (2015).
28. Y. Zhang, Q.-S. Meng, L. Zhang, Y. Luo, Y.-J. Yu, B. Yang, Y. Zhang, R. Esteban, J. Aizpurua, Y. Luo, J.-L. Yang, Z.-C. Dong, and J. Hou, "Sub-nanometre control of the coherent interaction between a single molecule and a plasmonic nanocavity," *Nat. Commun.* **8**(1), 15225 (2017).
29. M. Pelton, S. D. Storm, and H. Leng, "Strong coupling of emitters to single plasmonic nanoparticles: exciton-induced transparency and Rabi splitting," *Nanoscale* **11**(31), 14540–14552 (2019).
30. S. Corni and J. Tomasi, "Lifetimes of electronic excited states of a molecule close to a metal surface," *J. Chem. Phys.* **118**(14), 6481–6494 (2003).
31. O. Andreussi, S. Corni, B. Mennucci, and J. Tomasi, "Radiative and nonradiative decay rates of a molecule close to a metal particle of complex shape," *J. Chem. Phys.* **121**(20), 10190–10202 (2004).

32. T. Neuman, R. Esteban, D. Casanova, F. García-Vidal, and J. Aizpurua, "Coupling of molecular emitters and plasmonic cavities beyond the point-dipole approximation," *Nano Lett.* **18**(4), 2358–2364 (2018).
33. F. Aguilar-Galindo, S. Díaz-Tendero, and A. G. Borisov, "Electronic structure effects in the coupling of a single molecule with a plasmonic antenna," *J. Phys. Chem. C* **123**(7), 4446–4456 (2019).
34. Y. Zhang, Z.-C. Dong, and J. Aizpurua, "Influence of the chemical structure on molecular light emission in strongly localized plasmonic fields," *J. Phys. Chem. C* **124**(8), 4674–4683 (2020).
35. P. Song, P. Nordlander, and S. Gao, "Quantum mechanical study of the coupling of plasmon excitations to atomic-scale electron transport," *J. Chem. Phys.* **134**(7), 074701 (2011).
36. V. Kulkarni and A. Manjavacas, "Quantum effects in charge transfer plasmons," *ACS Photonics* **2**(7), 987–992 (2015).
37. P. Garcia-Gonzalez, A. Varas, F. Garcia-Vidal, and A. Rubio, "Single-atom control of the optoelectronic response in sub-nanometric cavities," arXiv preprint arXiv:1903.08443 (2019).
38. A. Babaze, R. Esteban, A. G. Borisov, and J. Aizpurua, "Electronic exciton–plasmon coupling in a nanocavity beyond the electromagnetic interaction picture," *Nano Lett.* **21**(19), 8466–8473 (2021).
39. A. Delga, J. Feist, J. Bravo-Abad, and F. Garcia-Vidal, "Quantum emitters near a metal nanoparticle: strong coupling and quenching," *Phys. Rev. Lett.* **112**(25), 253601 (2014).
40. M. V. Rybin, S. F. Mingaleev, M. F. Limonov, and Y. S. Kivshar, "Purcell effect and Lamb shift as interference phenomena," *Sci. Rep.* **6**(1), 20599 (2016).
41. P. Yao, C. Van Vlack, A. Reza, M. Patterson, M. Dignam, and S. Hughes, "Ultra-high Purcell factors and Lamb shifts in slow-light metamaterial waveguides," *Phys. Rev. B* **80**(19), 195106 (2009).
42. S. D'Agostino, F. Alpeggiani, and L. C. Andreani, "Strong coupling between a dipole emitter and localized plasmons: enhancement by sharp silver tips," *Opt. Express* **21**(23), 27602–27610 (2013).
43. E. M. Purcell, "Spontaneous emission probabilities at radio frequencies," in *Confined Electrons and Photons*, (Springer, 1995), pp. 839.
44. P. Apell and Å. Ljungbert, "Red shift of surface plasmons in small metal particles," *Solid State Commun.* **44**(9), 1367–1369 (1982).
45. C. Yannouleas and R. Broglia, "Landau damping and wall dissipation in large metal clusters," *Ann. Phys.* **217**(1), 105–141 (1992).
46. A. Liebsch, "Surface-plasmon dispersion and size dependence of Mie resonance: silver versus simple metals," *Phys. Rev. B* **48**(15), 11317–11328 (1993).
47. J. Pitarke, V. Silkin, E. Chulkov, and P. Echenique, "Theory of surface plasmons and surface-plasmon polaritons," *Rep. Prog. Phys.* **70**(1), 1–87 (2006).
48. T. V. Teperik, P. Nordlander, J. Aizpurua, and A. G. Borisov, "Quantum effects and nonlocality in strongly coupled plasmonic nanowire dimers," *Opt. Express* **21**(22), 27306–27325 (2013).
49. R. C. Monreal, T. J. Antosiewicz, and S. P. Apell, "Competition between surface screening and size quantization for surface plasmons in nanoparticles," *New J. Phys.* **15**(8), 083044 (2013).
50. E. Selenius, S. Malola, and H. Häkkinen, "Analysis of localized surface plasmon resonances in spherical jellium clusters and their assemblies," *J. Phys. Chem. C* **121**(48), 27036–27052 (2017).
51. J. Khurgin, W.-Y. Tsai, D. P. Tsai, and G. Sun, "Landau damping and limit to field confinement and enhancement in plasmonic dimers," *ACS Photonics* **4**(11), 2871–2880 (2017).
52. T. Perera, S. D. Gunapala, M. I. Stockman, and M. Premaratne, "Plasmonic properties of metallic nanoshells in the quantum limit: From single particle excitations to plasmons," *J. Phys. Chem. C* **124**(50), 27694–27708 (2020).
53. F. J. García de Abajo, "Nonlocal effects in the plasmons of strongly interacting nanoparticles, dimers, and waveguides," *J. Phys. Chem. C* **112**(46), 17983–17987 (2008).
54. W. Zhu, R. Esteban, A. G. Borisov, J. J. Baumberg, P. Nordlander, H. J. Lezec, J. Aizpurua, and K. B. Crozier, "Quantum mechanical effects in plasmonic structures with subnanometre gaps," *Nat. Commun.* **7**(1), 11495 (2016).
55. P. Gonçalves, T. Christensen, N. Rivera, A.-P. Jauho, N. A. Mortensen, and M. Soljačić, "Plasmon–emitter interactions at the nanoscale," *Nat. Commun.* **11**(1), 366 (2020).
56. N. A. Mortensen, "Mesoscopic electrodynamics at metal surfaces," *Nanophotonics* **10**(10), 2563–2616 (2021).
57. R. Fuchs and F. Claro, "Multipolar response of small metallic spheres: Nonlocal theory," *Phys. Rev. B* **35**(8), 3722–3727 (1987).
58. R. Ruppin, "Extinction properties of thin metallic nanowires," *Opt. Commun.* **190**(1–6), 205–209 (2001).
59. C. Ciraci, R. Hill, J. Mock, Y. Urzhumov, A. Fernández-Domínguez, S. Maier, J. Pendry, A. Chilkoti, and D. Smith, "Probing the ultimate limits of plasmonic enhancement," *Science* **337**(6098), 1072–1074 (2012).
60. G. Toscano, S. Raza, A.-P. Jauho, N. A. Mortensen, and M. Wubs, "Modified field enhancement and extinction by plasmonic nanowire dimers due to nonlocal response," *Opt. Express* **20**(4), 4176–4188 (2012).
61. L. Stella, P. Zhang, F. García-Vidal, A. Rubio, and P. García-González, "Performance of nonlocal optics when applied to plasmonic nanostructures," *J. Phys. Chem. C* **117**(17), 8941–8949 (2013).
62. Y. Luo, A. Fernandez-Dominguez, A. Wiener, S. A. Maier, and J. Pendry, "Surface plasmons and nonlocality: a simple model," *Phys. Rev. Lett.* **111**(9), 093901 (2013).
63. N. A. Mortensen, S. Raza, M. Wubs, T. Søndergaard, and S. I. Bozhevolnyi, "A generalized non-local optical response theory for plasmonic nanostructures," *Nat. Commun.* **5**(1), 3809 (2014).

64. C. David and F. J. García de Abajo, "Surface plasmon dependence on the electron density profile at metal surfaces," *ACS Nano* **8**(9), 9558–9566 (2014).
65. T. Christensen, W. Yan, S. Raza, A.-P. Jauho, N. A. Mortensen, and M. Wubs, "Nonlocal response of metallic nanospheres probed by light, electrons, and atoms," *ACS Nano* **8**(2), 1745–1758 (2014).
66. G. Toscano, J. Straubel, A. Kwiatkowski, C. Rockstuhl, F. Evers, H. Xu, N. A. Mortensen, and M. Wubs, "Resonance shifts and spill-out effects in self-consistent hydrodynamic nanoplasmonics," *Nat. Commun.* **6**(1), 7132 (2015).
67. S. Raza, S. I. Bozhevolnyi, M. Wubs, and N. A. Mortensen, "Nonlocal optical response in metallic nanostructures," *J. Phys. Cond. Matter* **27**(18), 183204 (2015).
68. C. Ciraci and F. Della Sala, "Quantum hydrodynamic theory for plasmonics: Impact of the electron density tail," *Phys. Rev. B* **93**(20), 205405 (2016).
69. C. Tserkezis, W. Yan, W. Hsieh, G. Sun, J. B. Khurgin, M. Wubs, and N. A. Mortensen, "On the origin of nonlocal damping in plasmonic monomers and dimers," *International Journal of Modern Physics B* **31**(24), 1740005 (2017).
70. M. Khalid, F. Della Sala, and C. Ciraci, "Optical properties of plasmonic core-shell nanomatryoshkas: a quantum hydrodynamic analysis," *Opt. Express* **26**(13), 17322–17334 (2018).
71. M. Kupresak, X. Zheng, G. A. Vandenbosch, and V. V. Moshchalkov, "Comparison of hydrodynamic models for the electromagnetic nonlocal response of nanoparticles," *Adv. Theory Simul.* **1**(12), 1800076 (2018).
72. H. M. Baghramyan, F. Della Sala, and C. Ciraci, "Laplacian-level quantum hydrodynamic theory for plasmonics," *Phys. Rev. X* **11**, 011049 (2021).
73. P. J. Feibelman, "Microscopic calculation of electromagnetic fields in refraction at a jellium–vacuum interface," *Phys. Rev. B* **12**(4), 1319–1336 (1975).
74. P. J. Feibelman, "Surface electromagnetic fields," *Prog. Surf. Sci.* **12**(4), 287–407 (1982).
75. P. Apell and Å. Ljungbert, "A general non-local theory for the electromagnetic response of a small metal particle," *Phys. Scr.* **26**(2), 113–118 (1982).
76. K. Kempa and W. L. Schaich, "Calculation of corrections to fresnel optics from density response," *Phys. Rev. B* **34**(2), 547–557 (1986).
77. W. Yan, M. Wubs, and N. A. Mortensen, "Projected dipole model for quantum plasmonics," *Phys. Rev. Lett.* **115**(13), 137403 (2015).
78. T. Christensen, W. Yan, A.-P. Jauho, M. Soljačić, and N. A. Mortensen, "Quantum corrections in nanoplasmonics: shape, scale, and material," *Phys. Rev. Lett.* **118**(15), 157402 (2017).
79. Y. Yang, D. Zhu, W. Yan, A. Agarwal, M. Zheng, J. D. Joannopoulos, P. Lalanne, T. Christensen, K. K. Berggren, and M. Soljačić, "A general theoretical and experimental framework for nanoscale electromagnetism," *Nature* **576**(7786), 248–252 (2019).
80. A. R. Echarri, P. A. D. Gonçalves, C. Tserkezis, F. J. García de Abajo, N. A. Mortensen, and J. D. Cox, "Optical response of noble metal nanostructures: quantum surface effects in crystallographic facets," *Optica* **8**(5), 710–721 (2021).
81. N. A. Mortensen, P. A. D. Gonçalves, F. A. Shuklin, J. D. Cox, C. Tserkezis, M. Ichikawa, and C. Wolff, "Surface-response functions obtained from equilibrium electron-density profiles," *Nanophotonics* **10**(14), 3647–3657 (2021).
82. P. Leung, "Decay of molecules at spherical surfaces: nonlocal effects," *Phys. Rev. B* **42**(12), 7622–7625 (1990).
83. M. Hider and P. Leung, "Nonlocal electrodynamic modeling of fluorescence characteristics for molecules in a spherical cavity," *Phys. Rev. B* **66**(19), 195106 (2002).
84. C. Tserkezis, N. Stefanou, M. Wubs, and N. A. Mortensen, "Molecular fluorescence enhancement in plasmonic environments: exploring the role of nonlocal effects," *Nanoscale* **8**(40), 17532–17541 (2016).
85. A. Vagov, I. Larkin, M. D. Croitoru, and V. M. Axt, "Role of nonlocality and landau damping in the dynamics of a quantum dot coupled to surface plasmons," *Phys. Rev. B* **93**(19), 195414 (2016).
86. R. Jurga, S. D'Agostino, F. Della Sala, and C. Ciraci, "Plasmonic nonlocal response effects on dipole decay dynamics in the weak-and strong-coupling regimes," *J. Phys. Chem. C* **121**(40), 22361–22368 (2017).
87. C. Tserkezis, N. A. Mortensen, and M. Wubs, "How nonlocal damping reduces plasmon-enhanced fluorescence in ultranarrow gaps," *Phys. Rev. B* **96**(8), 085413 (2017).
88. C. Tserkezis, M. Wubs, and N. A. Mortensen, "Robustness of the Rabi splitting under nonlocal corrections in plexcitonics," *ACS Photonics* **5**(1), 133–142 (2018).
89. C. Ciraci, R. Jurga, M. Khalid, and F. Della Sala, "Plasmonic quantum effects on single-emitter strong coupling," *Nanophotonics* **8**(10), 1821–1833 (2019).
90. V. Karanikolas, I. Thanopoulos, J. D. Cox, T. Kuroda, J.-i. Inoue, N. A. Mortensen, E. Paspalakis, and C. Tserkezis, "Quantum surface effects in strong coupling dynamics," *Phys. Rev. B* **104**(20), L201405 (2021).
91. T. V. Teperik, P. Nordlander, J. Aizpurua, and A. G. Borisov, "Robust subnanometric plasmon ruler by rescaling of the nonlocal optical response," *Phys. Rev. Lett.* **110**(26), 263901 (2013).
92. P. Zhang, J. Feist, A. Rubio, P. García-González, and F. García-Vidal, "Ab initio nanoplasmonics: The impact of atomic structure," *Phys. Rev. B* **90**(16), 161407 (2014).
93. E. B. Guidez and C. M. Aikens, "Quantum mechanical origin of the plasmon: from molecular systems to nanoparticles," *Nanoscale* **6**(20), 11512–11527 (2014).
94. M. Barbry, P. Koval, F. Marchesin, R. Esteban, A. G. Borisov, J. Aizpurua, and D. Sánchez-Portal, "Atomistic near-field nanoplasmonics: reaching atomic-scale resolution in nanooptics," *Nano Lett.* **15**(5), 3410–3419 (2015).

95. T. P. Rossi, A. Zugarramurdi, M. J. Puska, and R. M. Nieminen, "Quantized evolution of the plasmonic response in a stretched nanorod," *Phys. Rev. Lett.* **115**(23), 236804 (2015).
96. M. Zapata Herrera, J. Aizpurua, A. K. Kazansky, and A. G. Borisov, "Plasmon response and electron dynamics in charged metallic nanoparticles," *Langmuir* **32**(11), 2829–2840 (2016).
97. A. Varas, P. García-González, J. Feist, F. García-Vidal, and A. Rubio, "Quantum plasmonics: from jellium models to ab initio calculations," *Nanophotonics* **5**(3), 409–426 (2016).
98. D.-C. Marinica, J. Aizpurua, and A. G. Borisov, "Quantum effects in the plasmon response of bimetallic core-shell nanostructures," *Opt. Express* **24**(21), 23941–23956 (2016).
99. H.-C. Weissker, "Optical Properties of Noble Metal Clusters from the Ab Initio Perspective," in *Encyclopedia of Interfacial Chemistry*, K. Wandelt, ed. (Elsevier, 2018), pp. 546–558.
100. M. R. A. Barbry, "Plasmons in nanoparticles: atomistic ab initio theory for large systems," Ph.D. thesis, University of the Basque Country (2018).
101. G. Aguirregabiria, D.-C. Marinica, M. Ludwig, D. Brida, A. Leitenstorfer, J. Aizpurua, and A. G. Borisov, "Dynamics of electron-emission currents in plasmonic gaps induced by strong fields," *Faraday Discuss.* **214**, 147–157 (2019).
102. E. Townsend and G. W. Bryant, "Which resonances in small metallic nanoparticles are plasmonic?" *J. Opt.* **16**(11), 114022 (2014).
103. J. Zuloaga, E. Prodan, and P. Nordlander, "Quantum description of the plasmon resonances of a nanoparticle dimer," *Nano Lett.* **9**(2), 887–891 (2009).
104. R. Esteban, A. G. Borisov, P. Nordlander, and J. Aizpurua, "Bridging quantum and classical plasmonics with a quantum-corrected model," *Nat. Commun.* **3**(1), 825 (2012).
105. H. Duan, A. I. Fernández-Domínguez, M. Bosman, S. A. Maier, and J. K. Yang, "Nanoplasmonics: classical down to the nanometer scale," *Nano Lett.* **12**(3), 1683–1689 (2012).
106. F. Marchesin, P. Koval, M. Barbry, J. Aizpurua, and D. Sanchez-Portal, "Plasmonic response of metallic nanojunctions driven by single atom motion: quantum transport revealed in optics," *ACS Photonics* **3**(2), 269–277 (2016).
107. G. Aguirregabiria, D. C. Marinica, R. Esteban, A. K. Kazansky, J. Aizpurua, and A. G. Borisov, "Role of electron tunneling in the nonlinear response of plasmonic nanogaps," *Phys. Rev. B* **97**(11), 115430 (2018).
108. L. Novotny and B. Hecht, *Principles of nano-optics* (Cambridge university press, 2012).
109. A. F. Koenderink, "On the use of purcell factors for plasmon antennas," *Opt. Lett.* **35**(24), 4208–4210 (2010).
110. X. Zambrana-Puyalto and N. Bonod, "Purcell factor of spherical mie resonators," *Phys. Rev. B* **91**(19), 195422 (2015).
111. M. Brack, "The physics of simple metal clusters: self-consistent jellium model and semiclassical approaches," *Rev. Mod. Phys.* **65**(3), 677–732 (1993).
112. W. Ekardt, "Dynamical polarizability of small metal particles: self-consistent spherical jellium background model," *Phys. Rev. Lett.* **52**(21), 1925–1928 (1984).
113. E. Gross and W. Kohn, "Time-dependent density-functional theory," in *Density Functional Theory of Many-Fermion Systems, vol. 21 of Advances in Quantum Chemistry* P.-O. Löwdin, ed. (Academic Press, 1990), pp. 255–291.
114. R. O. Jones, "Density functional theory: Its origins, rise to prominence, and future," *Rev. Mod. Phys.* **87**(3), 897–923 (2015).
115. J. Friedel, "Xiv. the distribution of electrons round impurities in monovalent metals," *The London, Edinburgh, and Dublin Philosophical Magazine and Journal of Science* **43**(337), 153–189 (1952).
116. W. Kohn and L. J. Sham, "Quantum density oscillations in an inhomogeneous electron gas," *Phys. Rev.* **137**(6A), A1697–A1705 (1965).
117. D. Marinica, A. Kazansky, P. Nordlander, J. Aizpurua, and A. G. Borisov, "Quantum plasmonics: Nonlinear effects in the field enhancement of a plasmonic nanoparticle dimer," *Nano Lett.* **12**(3), 1333–1339 (2012).
118. O. Gunnarsson and B. I. Lundqvist, "Exchange and correlation in atoms, molecules, and solids by the spin-density-functional formalism," *Phys. Rev. B* **13**(10), 4274–4298 (1976).
119. M. Marques and E. Gross, "Time-dependent density functional theory," *Annu. Rev. Phys. Chem.* **55**(1), 427–455 (2004).
120. C. Leforestier, R. H. Bisseling, C. Cerjan, M. D. Feit, R. Friesner, A. Gulberg, A. Hammerich, G. Jolicard, W. Karrlein, H.-D. Meyer, N. Lipkin, O. Roncero, and R. Kosloff, "A comparison of different propagation schemes for the time dependent schrödinger equation," *J. Comput. Phys.* **94**(1), 59–80 (1991).
121. A. Babaze, R. Esteban, J. Aizpurua, and A. G. Borisov, "Second-harmonic generation from a quantum emitter coupled to a metallic nanoantenna," *ACS Photonics* **7**(3), 701–713 (2020).
122. H. O. Wijewardane and C. A. Ullrich, "Time-dependent kohn-sham theory with memory," *Phys. Rev. Lett.* **95**(8), 086401 (2005).
123. G. Vignale and W. Kohn, "Current-dependent exchange-correlation potential for dynamical linear response theory," *Phys. Rev. Lett.* **77**(10), 2037–2040 (1996).
124. M. Schmeits, "Surface-plasmon coupling in cylindrical pores," *Phys. Rev. B* **39**(11), 7567–7577 (1989).
125. M. Schmeits and L. Dambly, "Fast-electron scattering by bispherical surface-plasmon modes," *Phys. Rev. B* **44**(23), 12706–12712 (1991).
126. M. K. Svendsen, C. Wolff, A.-P. Jauho, N. A. Mortensen, and C. Tserkezis, "Role of diffusive surface scattering in nonlocal plasmonics," *J. Phys. Cond. Matter* **32**(39), 395702 (2020).



127. A. Delga, J. Feist, J. Bravo-Abad, and F. Garcia-Vidal, "Theory of strong coupling between quantum emitters and localized surface plasmons," *J. Opt.* **16**(11), 114018 (2014).
128. S. Raza, S. Kakhodazadeh, T. Christensen, M. Di Vece, M. Wubs, N. A. Mortensen, and N. Stenger, "Multipole plasmons and their disappearance in few-nanometre silver nanoparticles," *Nat. Commun.* **6**(1), 8788 (2015).
129. I. Romero, J. Aizpurua, G. W. Bryant, and F. J. G. de Abajo, "Plasmons in nearly touching metallic nanoparticles: singular response in the limit of touching dimers," *Opt. Express* **14**(21), 9988–9999 (2006).
130. P. Nordlander, C. Oubre, E. Prodan, K. Li, and M. Stockman, "Plasmon hybridization in nanoparticle dimers," *Nano Lett.* **4**(5), 899–903 (2004).
131. R. Kosloff, "Quantum molecular dynamics on grids," in *Dynamics of molecules and chemical reactions* (1996), pp. 185–230.